

HU ISSN 1586–2070

JOURNAL OF COMPUTATIONAL AND APPLIED MECHANICS

A Publication of the University of Miskolc

VOLUME 6, NUMBER 2 (2005)



MISKOLC UNIVERSITY PRESS

HU ISSN 1586–2070

JOURNAL OF COMPUTATIONAL AND APPLIED MECHANICS

A Publication of the University of Miskolc

VOLUME 6, NUMBER 2 (2005)



MISKOLC UNIVERSITY PRESS

EDITORIAL BOARD

- István PÁCZELT, Editor in Chief, Department of Mechanics, University of Miskolc, 3515 MISKOLC, Hungary, mechpacz@uni-miskolc.hu
- László BARANYI, Department of Fluid and Heat Engineering, University of Miskolc, 3515 MISKOLC, Hungary, aramb1@uni-miskolc.hu
- Edgár BERTÓTI, Department of Mechanics, University of Miskolc, 3515 MISKOLC, Hungary, mechber@uni-miskolc.hu
- Tibor CZIBERE, Department of Fluid and Heat Engineering, University of Miskolc, 3515 MISKOLC, Hungary, aramct@uni-miskolc.hu
- István ECSEDI, Department of Mechanics, University of Miskolc, 3515 MISKOLC, Hungary, mechecs@uni-miskolc.hu
- Wolfram FRANK, Institut für Fluid- und Thermodynamik, Universität Siegen, Paul-Bonatz-Strasse 9-11, 57076 SIEGEN, Germany, frank@ift.mb.uni-siegen.de
- Ulrich GABBERT, Institut für Mechanik, Otto-von-Guericke-Universität Magdeburg, Universitätsplatz 2, 39106 MAGDEBURG, Germany, ulrich.gabbert@mb.uni-magdeburg.de
- Zolt GÁSPÁR, Department of Structural Mechanics, Budapest University of Technology and Economics, Műegyetem rkp. 3, 1111 BUDAPEST, Hungary, gaspar@ep-mech.me.bme.hu
- Robert HABER, Department of Theoretical and Applied Mechanics, University of Illinois at Urbana-Champaign, 216 Talbot Lab., 104 S. Wright Str., URBANA, IL 61801, USA, r-haber@uiuc.edu
- Gábor HALÁSZ, Department of Hydraulic Machines, Budapest University of Technology and Economics, Műegyetem rkp. 3, 1111 BUDAPEST, Hungary, HALASZ@vizgep.bme.hu
- Ji Huan HE, Department of Mathematics, College of Basic Science, Shanghai Donghua University, No. 1882 Yan'anxilu Road, 200051 SHANGHAI, China, jhhe@dhu.edu.cn
- Károly JÁRMAI, Department of Materials Handling and Logistics, University of Miskolc, 3515 MISKOLC, Hungary, altjar@gold.uni-miskolc.hu
- László KOLLÁR, Department of Strength of Materials and Structures, Budapest University of Technology and Economics, Műegyetem rkpt. 1-3. K.II.42., 1521 BUDAPEST, Hungary, lkollar@goliat.eik.bme.hu
- Vladimir KOMPIŠ, Department of Mechanics, University of Žilina, ŽILINA, Slovakia, Vladimir_Kompis@kmpp.utc.sk
- Imre KOZÁK, Department of Mechanics, University of Miskolc, 3515 MISKOLC, Hungary, mechkoz@uni-miskolc.hu
- József KÖVECSÉS, Department of Mechanical Engineering, McGill University, 817 Sherbrooke Street West, MD163, Montreal, Quebec H3A 2K6, jozsef.kovecses@mcgill.ca
- Márta KURUTZ, Department of Structural Mechanics, Budapest University of Technology and Economics, Műegyetem rkp. 3, 1111 BUDAPEST, Hungary, kurutzm@eik.bme.hu
- R. Ivan LEWIS, Room 2-16 Bruce Building, Newcastle University, NEWCASTLE UPON TYNE, NE1 7RU, UK, R.I.Lewis@NCL.AC.UK
- Gennadij LVOV, Department of Mechanics, Kharkov Polytechnical Institute, 2 Frunze Str., 310002 KHARKOV, Ukraine, lvovgi@kpi.kharkov.ua
- Herbert MANG, Institute for Strength of Materials, University of Technology, Karlsplatz 13, 1040 VIENNA, Austria, Herbert.Mang@tuwien.ac.at
- Zenon MROZ, Polish Academy of Sciences, Institute of Fundamental Technological Research, Swietokrzyska 21, WARSAW, Poland, zmroz@ippt.gov.pl
- Tibor NAGY, Department of Physics, University of Miskolc, 3515 MISKOLC, Hungary, fiznagyt@uni-miskolc.hu
- Gyula PATKÓ, Department of Machine Tools, University of Miskolc, 3515 MISKOLC, Hungary, mechpgy@uni-miskolc.hu
- Jan SLADEK, Ústav stavbenictva a architektúry, Slovenskej akadémie vied, Dubróvska cesta 9, 842 20 BRATISLAVA, Slovakia, usarslad@savba.sk
- Gábor STÉPÁN, Department of Mechanics, Budapest University of Technology and Economics, Műegyetem rkp. 3, 1111 BUDAPEST, Hungary, stepan@mm.bme.hu
- Barna SZABÓ, Center for Computational Mechanics, Washington University, Campus Box 1129, St. LOUIS, MO63130, USA, szabo@ccm.wustl.edu
- Szilárd SZABÓ, Department of Fluid and Heat Engineering, University of Miskolc, 3515 MISKOLC, Hungary, aram2xsz@uni-miskolc.hu
- György SZEIDL, Department of Mechanics, University of Miskolc, 3515 MISKOLC, Hungary, Gyorgy.SZEIDL@uni-miskolc.hu

LOCAL EDITORIAL COUNCIL

T. CZIBERE, I. KOZÁK, I. PÁCZELT, G. PATKÓ, G. SZEIDL

GENERALIZED MINDLIN'S METHOD FOR THE DETERMINATION OF CONSTITUTIVE EQUATIONS OF SOLIDS

GYULA BÉDA

Department of Applied Mechanics
Budapest University of Technology and Economics
Műegyetem rkp. 3, 1111 BUDAPEST, Hungary
beda@math.uni-potsdam.de

[Received: December 14, 2004]

Dedicated to István Páczelt on the occasion of his 65th birthday

Abstract. For solid bodies the principle of virtual work can often be written as the variation of a functional. This fact can be applied to determine constitutive equations. Mindlin utilized this idea in the determination of higher order constitutive equations. Mindlin's method can be generalized into a few directions. Such generalizations result in that the first order constitutive equations contain first derivatives of strain and stress with respect to time and space coordinates in a linear form only.

Mathematical Subject Classification: 74A20, 74A35

Keywords: Lagrange's derivative, evolution equation, Lagrange's derivative with condition, constitutive equation

1. Introduction

The variational principles of solids contain expressions

$$\int_{t_0}^{t_1} \int_V \boldsymbol{\sigma} \cdot \cdot \delta \boldsymbol{\varepsilon} \, dV dt \quad \text{or} \quad \int_{t_0}^{t_1} \int_V \boldsymbol{\varepsilon} \cdot \cdot \delta \boldsymbol{\sigma} \, dV dt.$$

Remaining at the first expression the identity

$$\int_{t_0}^{t_1} \int_V \boldsymbol{\sigma} \cdot \cdot \delta \boldsymbol{\varepsilon} \, dV dt \equiv \delta \int_{t_0}^{t_1} \int_V W(\cdot) \, dV dt$$

is frequently encountered. This expression can also be written in the generalized form

$$\int_{t_0}^{t_1} \int_V \boldsymbol{\sigma} \cdot \cdot \delta \boldsymbol{\varepsilon} \, dV dt = \int_{t_0}^{t_1} \int_V [\delta U(\cdot) + \mathbf{D}(\cdot) \cdot \cdot \delta \boldsymbol{\varepsilon}] \, dV dt.$$

Function \mathbf{D} is not known generally and it will be abandoned in the following.

The stresses, strains and the variation of strains are denoted by $\boldsymbol{\sigma}$, $\boldsymbol{\varepsilon}$ and $\delta \boldsymbol{\varepsilon}$, respectively. Double dots stand for the double scalar product.

Mindlin [2] investigated equation

$$\int_V \boldsymbol{\sigma} \cdot \cdot \delta \boldsymbol{\varepsilon} \, dV = \delta \int_V W(\boldsymbol{\varepsilon}, \boldsymbol{\varepsilon} \nabla, \boldsymbol{\varepsilon} \nabla \nabla) \, dV,$$

where the function W depends on the strains $\boldsymbol{\varepsilon}$, the strain gradient $\boldsymbol{\varepsilon} \nabla$ and the gradient of the strain gradient $\boldsymbol{\varepsilon} \nabla \nabla$. The variables of the scalar function W are second, third and fourth order tensors.

The present paper generalizes Mindlin's idea making use of time derivatives and the existence of acceleration waves in solids [1] (*first condition*). In order to simplify the problem small deformations will be assumed and uniaxial stress and strain states will be investigated.

2. Lagrange derivative

In case of uniaxial problems the strain ε and the stress σ depend on the space and time coordinates x and t . Dash and dot denote the spatial and time derivatives.

For the uniaxial case we shall assume that the function W takes the following form

$$W(\varepsilon, \sigma, \dot{\varepsilon}, \dot{\sigma}, \varepsilon', \sigma').$$

It follows from this representation that

$$\begin{aligned} \int_{t_0}^{t_1} \int_{x_0}^{x_1} \sigma \delta \varepsilon \, dx \, dt &= \delta \int_{t_0}^{t_1} \int_{x_0}^{x_1} W(\varepsilon, \sigma, \dot{\varepsilon}, \dot{\sigma}, \varepsilon', \sigma') \, dx \, dt \\ &\equiv \int_{t_0}^{t_1} \int_{x_0}^{x_1} \mathcal{L}_\varepsilon(W) \delta \varepsilon \, dx \, dt, \end{aligned} \quad (1)$$

where \mathcal{L}_ε denotes the Lagrange derivative of W with respect to ε , that is,

$$\mathcal{L}_\varepsilon(W) = \frac{\partial W}{\partial \varepsilon} - \left(\frac{\partial W}{\partial \dot{\varepsilon}} \right)' - \left(\frac{\partial W}{\partial \varepsilon'} \right)'.$$

Similarly, the Lagrange's derivative of W with respect to σ , reads

$$\mathcal{L}_\sigma(W) = \frac{\partial W}{\partial \sigma} - \left(\frac{\partial W}{\partial \dot{\sigma}} \right)' - \left(\frac{\partial W}{\partial \sigma'} \right)'.$$

Formula (1) yields that

$$\sigma = \mathcal{L}_\varepsilon(W), \quad (2)$$

and similarly

$$\varepsilon = \mathcal{L}_\sigma(W). \quad (3)$$

Mindlin has determined the stress for finite deformation [2]. If the strains are small and $W = W(\varepsilon, \varepsilon', \varepsilon'')$, we have

$$\sigma = \mathcal{L}_\varepsilon(W) = \frac{\partial W}{\partial \varepsilon} - \left(\frac{\partial W}{\partial \varepsilon'} \right)' - \left(\frac{\partial W}{\partial \varepsilon''} \right)''$$

or in detail

$$\begin{aligned} \sigma = & \frac{\partial W}{\partial \varepsilon} - \frac{\partial^2 W}{\partial \varepsilon' \partial \varepsilon} \varepsilon' - \frac{\partial^2 W}{\partial \partial \varepsilon'^2} \varepsilon'' - \frac{\partial^2 W}{\partial \varepsilon' \partial \varepsilon''} \varepsilon''' \\ & + \frac{\partial^2 W}{\partial \varepsilon'' \partial \varepsilon} \varepsilon'' + \frac{\partial^2 W}{\partial \varepsilon'' \partial \varepsilon'} \varepsilon''' + \frac{\partial^2 W}{\partial \varepsilon''^2} \varepsilon^{iv} . \end{aligned} \quad (4)$$

Supposing that the formulation (4) does not contain higher derivatives, i.e., it involves first derivatives only then the derivatives of W are zero with respect to ε'' and ε'^2 (second condition). Therefore W assumes the form

$$W = U(\varepsilon) + D(\varepsilon) \varepsilon'.$$

The stress σ can be derived from the function W as

$$\sigma = \frac{\partial U}{\partial \varepsilon} + \frac{\partial D}{\partial \varepsilon} \varepsilon' - \frac{\partial D}{\partial \varepsilon} \varepsilon' = \frac{\partial U}{\partial \varepsilon},$$

which means that the body is Green's elastic body.

3. Generalizations of Mindlin's method

3.1. The variables extension. We shall seek the constitutive equation in the following form

$$f(\varepsilon, \sigma, \dot{\varepsilon}, \dot{\sigma}, \varepsilon', \sigma') = 0. \quad (5)$$

(a) Let us set

$$W = A(\varepsilon) \varepsilon' + B(\varepsilon) \dot{\varepsilon}.$$

Since the Lagrange derivative of W is equal to zero, that is

$$\sigma = \mathcal{L}_\varepsilon(W) = 0,$$

it follows that there exists no constitutive equation.

(b) If

$$W_1 = A_1(\varepsilon, \sigma) + B_1(\varepsilon, \sigma) \varepsilon'$$

is given, then the stress is

$$\sigma = \mathcal{L}_\varepsilon(W) = \frac{\partial A_1}{\partial \varepsilon} - \frac{\partial B_1}{\partial \sigma} \sigma'.$$

Similarly, if W is equal to

$$A_2(\varepsilon, \sigma) + B_2(\varepsilon, \sigma) \dot{\varepsilon},$$

the stress is of the form

$$\sigma = \mathcal{L}_\varepsilon(W) = \frac{\partial A_2}{\partial \varepsilon} - \frac{\partial B_2}{\partial \sigma} \dot{\sigma}.$$

The two constitutive equations are $f_1(\varepsilon, \sigma, \sigma') = 0$ and $f_2(\varepsilon, \sigma, \dot{\sigma}) = 0$. However neither the first equation nor the second one are constitutive equations because the first condition is not satisfied [1].

- (c) The second condition also excludes equation (5) from the set of possible constitutive equations. Namely the function W in this case reads

$$W = A(\varepsilon, \sigma) + B(\varepsilon, \sigma) \dot{\varepsilon} + C(\varepsilon, \sigma) \varepsilon' + D(\varepsilon, \sigma) \dot{\sigma} + E(\varepsilon, \sigma) \sigma' .$$

Consequently, the corresponding stress has the form

$$\sigma = \mathcal{L}_\varepsilon(W) = \frac{\partial A}{\partial \varepsilon} + \left(\frac{\partial D}{\partial \varepsilon} - \frac{\partial B}{\partial \sigma} \right) \dot{\sigma} + \left(\frac{\partial E}{\partial \varepsilon} - \frac{\partial C}{\partial \sigma} \right) \sigma' .$$

This equation does not satisfy the first condition, that is there exist no acceleration wave.

The results of these investigations have led to the conclusion that the function σ depends on either the strain ε or $\dot{\varepsilon}$ and also on the first or the second or the higher derivatives of the strain and stress. The present paper does not deal with higher order constitutive equations of this type.

3.2. Internal variables. Another way to generalize Mindlin's method is the introduction of an internal variable or internal variables. For example, assume that function W depends on $\varepsilon, \dot{\varepsilon}, \varepsilon'$ and the internal variable g . That is $W = W(\varepsilon, \dot{\varepsilon}, \varepsilon', g)$. An evolution equation should be written for the internal variable. Let the evolution equation be

$$G(\varepsilon, \sigma) \frac{\partial g}{\partial \dot{\sigma}} + \frac{\partial g}{\partial \dot{\varepsilon}} = 0 . \quad (6)$$

Equation (6) is the necessary condition of the existence of acceleration waves.

The Lagrange derivative of function W is

$$\mathcal{L}_\varepsilon(W) = \frac{\partial W}{\partial \varepsilon} - \left(\frac{\partial^2 W}{\partial \dot{\varepsilon} \partial \varepsilon} \dot{\varepsilon} + \frac{\partial^2 W}{\partial \varepsilon' \partial \varepsilon} \varepsilon' + \frac{\partial^2 W}{\partial \dot{\varepsilon} \partial g} \dot{g} + \frac{\partial^2 W}{\partial \varepsilon' \partial g} g' + (()) \right), \quad (7)$$

where $(())$ contains the higher derivatives of the variables ε and g . Term $(())$ will be omitted in view of the second condition. Evolution equation (6) implies that internal variable g depends on $\varepsilon, \sigma, \dot{\varepsilon}, \dot{\sigma}$, that is,

$$g = g(\varepsilon, \sigma, \dot{\varepsilon}, \dot{\sigma}) .$$

Now the following equation can be written

$$W = A(\varepsilon, g) + B(\varepsilon, g) \dot{\varepsilon} + C(\varepsilon, g) \varepsilon' .$$

Equation (6) is satisfied if

$$g = \sigma \quad \text{and} \quad G(\varepsilon, \sigma) \frac{\partial B}{\partial \sigma} + \frac{\partial B}{\partial \varepsilon} = 0 .$$

Finally, the stress σ is of the form (see equation (7))

$$\sigma = \frac{\partial A}{\partial \varepsilon} - \frac{\partial B}{\partial \varepsilon} \dot{\varepsilon} - \frac{\partial B}{\partial \sigma} \dot{\sigma} - \frac{\partial C}{\partial \varepsilon} \varepsilon' - \frac{\partial C}{\partial \sigma} \sigma' .$$

3.3. Conditional Lagrange derivative. A further generalization of the method can be made if we define a conditional Lagrange derivative. Then the Lagrange derivative of function W should be formed in such a way that equation $K = 0$ is also satisfied. Then we can calculate the Lagrange derivative of function $F = W + \lambda K$: Here λ is an arbitrary function, which depends on x and t .

Assume that the equation $K = 0$ coincides with equation (6). Then the function F reads

$$F = W(\varepsilon, \sigma, \dot{\varepsilon}, \varepsilon', \dot{\sigma}, \sigma') + \lambda(x, t) K(\varepsilon, \sigma, \dot{\varepsilon}, \dot{\sigma}),$$

where

$$K = G(\varepsilon, \sigma) \frac{\partial g}{\partial \dot{\sigma}} + \frac{\partial g}{\partial \dot{\varepsilon}} = 0.$$

After all that has been said, we get

$$\sigma = \mathcal{L}_\varepsilon(W) + \lambda \mathcal{L}_\varepsilon(K), \quad \text{if } K = 0. \quad (8)$$

Since now the second condition is satisfied, the function W is of the form

$$W = A(\varepsilon, \sigma) + B(\varepsilon, \sigma) \dot{\varepsilon} + C(\varepsilon, \sigma) \varepsilon' + D(\varepsilon, \sigma) \dot{\sigma} + E(\varepsilon, \sigma) \sigma'.$$

From this expression one can determine the derivative $\mathcal{L}_\varepsilon(W)$. As is well known, the derivative $\mathcal{L}_\varepsilon(K)$ is

$$\mathcal{L}_\varepsilon(K) = \frac{\partial K}{\partial \varepsilon} - \left(\frac{\partial^2 K}{\partial \dot{\varepsilon} \partial \varepsilon} \dot{\varepsilon} + \frac{\partial^2 K}{\partial \dot{\varepsilon} \partial \sigma} \dot{\sigma} \right).$$

The stress σ follows from equation (8), that is

$$\begin{aligned} \sigma &= \frac{\partial A}{\partial \varepsilon} + \lambda \frac{\partial K}{\partial \varepsilon} - \left(\frac{\partial D}{\partial \varepsilon} - \frac{\partial B}{\partial \sigma} + \lambda \frac{\partial^2 K}{\partial \dot{\varepsilon} \partial \sigma} \right) \dot{\sigma} \\ &\quad - \lambda \frac{\partial^2 K}{\partial \dot{\varepsilon} \partial \varepsilon} \dot{\varepsilon} - \left(\frac{\partial E}{\partial \varepsilon} - \frac{\partial C}{\partial \sigma} \right) \sigma'. \end{aligned}$$

The sufficient condition for the existence of an acceleration wave in continua is [1]

$$\frac{\lambda \frac{\partial^2 K}{\partial \dot{\varepsilon} \partial \varepsilon}}{\frac{\partial D}{\partial \varepsilon} - \frac{\partial B}{\partial \sigma} + \lambda \frac{\partial^2 K}{\partial \dot{\varepsilon} \partial \sigma}} < 0.$$

The necessary condition that satisfies it is equation (6).

4. Conclusions

Mindlin's method for the determination of constitutive equations can be generalized in several directions. The method of extension of the variables does not lead to new constitutive equation if the first derivatives of stress and strain can occur in the constitutive equations. This investigation directs attention to higher order constitutive equations. The other two generalizations can lead to possible constitutive equations.

Acknowledgement. This work was supported by the National Scientific Research Fund of Hungary (under contract OTKA T037715). This support is gratefully acknowledged.

References

1. BÉDA, GY.: Die Differentialgleichungen der möglichen Stoffgesetze des dynamischen plastischen Zuges. *Publications of the Technical University of Miskolc*, **25**, (1965), 194-204.
2. MINDLIN, R.D.: Second gradient of strain and surface-tension in linear elasticity. *International Journal of Solids Structures*, **1**, (1965), 417-438.

EVOLUTION METHODS FOR DISCRETE MINIMAL WEIGHT DESIGN OF SPACE TRUSSES WITH STABILITY CONSTRAINTS

ANIKÓ CSÉBFALVI

Department of Structural Engineering

University of Pécs

Boszorkány u. 2., 7624 Pécs, Hungary

csebfalv@witch.pmmf.hu

[Received: January 14, 2005]

Dedicated to István Páczelt on the occasion of his 65th birthday

Abstract. This paper provides a comparative study of evolution methods for minimal weight design of space trusses. Recently used genetic algorithms (GA), simulated annealing (SA) and tabu search (TS) methods are observed for metal structures where the truss member profiles are selected from available catalogue values. In this paper, global and local stability problems are considered using a path-following method for non-linear stability investigation. The results of the comparative study are presented for the commonly known numerical test problems. A twenty-four-member shallow dome structure was presented where structural instability constraints and member buckling are considered as well as using linear elastic material property. The effect of the nonlinear material law is compared in optimal design of the ten-bar truss structure and the twenty-five-bar transmission tower using an inverse Ramberg-Osgood material law.

Mathematical Subject Classification: 74P05

Keywords: evolution methods, minimal weight design of space trusses

1. Introduction

One of the most important practical considerations in the optimal design of steel structures is the best selection of design variables from available catalogue values. Therefore, the design is formulated as a discrete optimization problem, searching for global or local optimal solution. However, most optimization methods are suited and developed for continuous design variables. A few procedures [1, 3, 4, 5, 9, 13] have been considered for discrete optimization including e.g. enumeration techniques, integer programming, branch and bound algorithms.

This paper provides a comparative study where simulated annealing (SA), genetic algorithms (GA), and tabu search methods (TS) are considered for discrete minimal weight design problems of shallow space trusses with stability constraints.

Simulated annealing as a heuristic algorithm is associated with its original use for solving metal models as they heat and cool. Kirkpatrick et al. [10] introduced it first for discrete optimization problems. In this paper a new SA algorithm is presented for shallow space trusses with stability constraints. The SA algorithm has proven to be a good technique [6, 11] for solving combinatorial optimization problems in particular for large flexible space structures. However, it seems sometimes less useful than some conventional algorithms. Consequently, simulated annealing has not been widely accepted in engineering optimization. In order to accelerate the overall convergence, it is proposed to use the best solution for a starting point every time that the temperature is reduced. The results show that simulated annealing algorithm provides a computationally efficient tool to find near optimal solutions to otherwise computationally intractable problems.

GA methods are search algorithms that are based on the concepts of natural selection and natural genetics. Recently GA methods are very popular and have been used for sizing, shape, and topology optimization of structures, e.g. [8, 12]. The core characteristics of GAs are based on the principles of survival of the fittest and adaptation. GA methods operate on population of design variable sets, with each design variable set defining a potential solution called a string. Each string is made up of series of characters as binary numbers, representing the discrete variables for a particular solution. The fitness of each string is a measure of performance of design variables defined by the objective function and constraints. GA methods consist of a series of three processes: coding and decoding design variables into strings, evaluating the fitness of each solution string, and applying genetic operators to generate the next generation of solution strings. Most GA methods are variations of the simple GA proposed by Goldberg [8], which consists of three basic genetic operators: reproduction, crossover, and mutation. By varying these parameters, the convergence of the problem may be altered. Much attention has been focused on finding the theoretical relationships between these parameters. Rajeev and Krishnamoorthy [12] applied GA for optimal truss design. They presented all the computations for three successive generations in the form of tables for easy understanding of the problem. In this study a GA method is proposed for minimal weight design of trusses. According to the shallow space form, the instability consideration is required. The general procedure is described in subsection 3.2.

Tabu search (TS) is a computational process which attempts to solve difficult combinatorial optimization problems through controlled randomization. In other words, TS is a metaheuristic method designed to find near optimal solutions of combinatorial optimization problems. Basically it consists of several elements called the move, neighborhood, initial solution, searching strategy, intensification, diversification and stopping rules. For obtaining near optimum solutions of such problems, a better minimum of an objective function should be searched for among a huge number of local minimums, since it is almost impossible to find an exact optimum. 'Intensification' means decreasing of the objective function value to find a better solution closer to the local minimum. 'Diversification' means a jump from a searching region to other

regions to avoid getting trapped in a single local minimum. The details of the TS process are presented in paper [7] and in subsection 3.3.

2. Structural optimization problem

The basic, initial equation system of discrete minimal weight design is the total potential energy function of the geometrically nonlinear truss structure.

$$V(u_i, a_q, \lambda) = U(u_i(a_q)) - \lambda p_i u_i, \quad i = 1, 2, \dots, n \quad q = 1, 2, \dots, e \quad (1)$$

The total potential energy function is formulated in terms of load intensity parameter λ , applied external load vector p_i , nodal displacement vector u_i , and vector of the member sizing a_q , where n is the number of nodes, e is the number of elements, and $U(u_i(a_q))$ is the non-linear strain energy function. In this study nonlinear material is supposed in comparison with the results obtained by using the linear elastic material law. In the case of the nonlinear (Ramberg-Osgood) material law, the strain energy function $U(u_i(a_q))$ is replaced by the following expression:

$$U(u_i) = \frac{\sigma_y^2 \sqrt{\left(1 + \frac{E^2 \varepsilon_q^2(u_i)}{\sigma_y^2}\right)}}{E} - \frac{\sigma_y^2}{E}, \quad (2)$$

where E is the elasticity modulus, ε_q is the member strain, and σ_y is the yield stress of the materials applied.

The design variables are selected from a discrete set of the predetermined cross-sectional areas, such that minimize the total weight of the structure:

$$V(a_q) \longrightarrow \min \quad (3)$$

subject to

$$V_{,i} = 0 \quad (4)$$

$$\lambda(a_q) = 1 \quad (5)$$

$$i = 1, 2, \dots, n \quad q = 1, 2, \dots, e$$

where $V_{,i} = 0$ is the equilibrium criterion, $\lambda(a_q) = 1$ the maximal locally and globally stable and stress feasible load intensity. The path-following procedure of instability investigation is terminated when the unit load intensity is reached without any constraint violation.

The proposed instability investigation [2] is based on the perturbation technique of the stability theory and on the non-linear modification of the classical linear homotopy method. With the help of the higher-order predictor-corrector algorithm, we are able to compute an arbitrary load deflection path and detect the different types of stability points. Within the predictor step, we compute the solution of an implicit ODE problem and the corrector phase is the solution of a nonlinear equation system. The first-order derivatives are obtained from the equation system by null-space computation of the augmented Hessian matrix. The higher order derivatives are obtained from the inhomogeneous equations using the Moor-Penrose pseudo-inverse.

The basic function of the stability investigation is the total potential energy function. The equilibrium equation system is obtained from the total potential energy function. Starting from the zero point of the equilibrium path assuming that the Hessian is positive definite, the solution is obtained in terms of the arch-length parameter of the equilibrium path t .

The stability investigation is based on the eigenvalue computation of the Hessian matrix $V_{,ij}$. In every step of the path-following process we get information about the displacement, stresses, local, and global stability of the structure. This higher order predictor-corrector method provides an accurate computation of the singular points. It is capable of computing not only points but also segments of the equilibrium path. The curve segment approximation is the basis for the identification of the singular points. Since we are concerned with finding feasible designs we must define a certain appropriate measure of performance. In the proposed path-following approach the applied measure of design infeasibility $\lambda(a_q)$ is defined as the solution of the following system:

$$\lambda(a_q, t) \longrightarrow \max \quad (6)$$

$$0 \leq \lambda(a_q, t) \leq 1 \quad (7)$$

$$\eta_i(a_q, t) > 0 \quad (8)$$

$$\underline{s} \leq s_q(a_q, t) \leq \bar{s} \quad (9)$$

$$i = 1, 2, \dots, n \quad q = 1, 2, \dots, e$$

where t is the arch-length parameter of the equilibrium path, η_i is the vector of eigenvalues of Hessian matrix $V_{,ij}$, and \underline{s} , \bar{s} are the lower and upper bounds of the stress constraints.

The path-following process is terminated at the first constraint violation.

3. Discrete optimization methods

In this study tree heuristic techniques are considered: simulated annealing, a genetic algorithm and a tabu search method to find a solution for the discrete minimal weight design problem of shallow space trusses.

3.1. Simulated annealing. Simulated annealing is a computational process, which attempts to solve difficult combinatorial optimization problems through controlled randomization. Simulated annealing emulates the physical process of annealing which attempts to force a system to its lowest energy state through controlled cooling.

In general, the annealing process involves the following steps:

- The temperature of the system is raised to a sufficient level.
- The temperature of the system is maintained at the level for a prescribed amount of time.
- The system is allowed to cool under controlled conditions until the desired energy-state is attained.

The initial temperature the time system remains at and the rate at which the system is cooled are referred to as the annealing schedule. If the system is allowed to cool too fast it may freeze at an undesirable high-energy state. In simulated annealing the process starts at a given feasible or unfeasible solution. To avoid freezing at a local optimum the algorithm walks very slowly through the solution space.

The general procedure for the simulated annealing algorithm can be described as follows:

```

MaxStep = 1000
MaxNode = 150
MaxNeighbourhoodSearch = 10
Call ProblemDefinition
Temperature = 1
CoolingRatio = 0.95
n = 0
Call RandomInitialStructure
Call PathFollowingMethod
Call CurrentNodeUpdate
Call BestSolutionUpdate
Call BestFeasibleSolutionUpdate
For s = 1 To MaxStep
  ParentSolution = BestSolution
  For m = 1 To MaxNeighbourhoodSearch
    If RandomNeighbourStructure(ParentSolution)
  Then
    Call PathFollowingMethod
    If AcceptedSolution(Temperature) then
      n = n + 1
      Call CurrentNodeUpdate
      Call BestSolutionUpdate
      Call BestFeasibleSolutionUpdate
    Endif
  Else
    Exit
  End If
  Next m
  Call TemperatureUpdate: If Temperature < 0.001
  Then Exit
  Next s

```

3.2. Genetic algorithm. The genetic algorithm (GA) is an efficient and widely applied global search procedure based on a stochastic approach. All of the recently applied genetic algorithms for structural optimization have demonstrated that genetic algorithms can be powerful design tools [8, 12]. The crossover operation creates variations in the solution population by producing new solution strings that consist of parts taken from selected parent solution strings. The mutation operation introduces

random changes in the solution population. In GA, the mutation operation can be beneficial in reintroducing diversity in a population. In this study, a pair of parent solutions is randomly selected, with a higher probability of selection being ascribed to superior solutions. The two parents are combined using a crossover scheme that attempts to merge the strings representing them in a suitable fashion to produce an offspring solution. Offspring can also be modified by some random mutation perturbation. The algorithm selects the fittest solution of the current solution set, i.e. those with the best objective function values. Each pair of strings reproduces two new strings using a crossover process and then dies.

The steps of the algorithm:

```

PopulationSize = 50
NumberOfNewGenerations=50
CrossoverProbability=0.5
SwapProbability=0.1
MutationProbability=0.1
Call ProblemDefinition
Call RandomInitialPopulationGeneration
Call BestFeasibleSolutionUpdate
For n = 1 to NumberOfNewGenerations
  {i, j} ← Call RandomFittestParentPairSelection
  Call Crossover
  For Each Child: Call Mutation
    Call PathFollowingMethod
    Call BestFeasibleSolutionUpdate
  {i, j} ← Call OffspringPairUpdate
Next n

```

3.3. Tabu search algorithm. In the case of tabu search, diversification is introduced as follows: if there are no improving moves, the move that least degrades the objective function is chosen. In order to avoid returning to the local optimum just visited, the reverse moves are forbidden. This is realized by storing those moves in a data structure called the tabu list. This contains s elements, which define forbidden moves, where s is the tabu list size. Once a move is stored in the tabu list, it will become available s iterations later.

The steps of the algorithm:

```

MaxStep = 1000
MaxNode=150
MaxNeighbourhoodSearch = 10
MaxTabuListSize=50
Call ProblemDefinition
n = 0
Call RandomInitialStructure

```

```

Call CurrentNodeUpdate
Call BestFeasibleSolutionUpdate
Call BestNodeUpdate
For s= 1 To MaxStep
    ParentSolution = BestSolution
    For m = 1 To MaxNeighbourhoodSearch
        If RandomNeighbourStructure(ParentSolution)
    Then
        n=n+1
        Call PathFollowingMethod
        Call BestFeasibleSolutionUpdate
        Call CurrentNodeUpdate
        Call BestNodeUpdate
        If n = MaxNode then Exit
    Else
        Exit
    End If
Next m
Next s

```

4. Numerical example

4.1. **The 24-member dome structure.** In this paper, one of the frequently used test examples is considered. The geometry of the 24-member is shown in Figure 1 and Table 1. According to the requirement of the symmetrical structure, the truss members were partitioned into linking groups. Group 1 includes bars 1-6, group 2 includes bars 7-12, and group 3 includes bars 13-24.

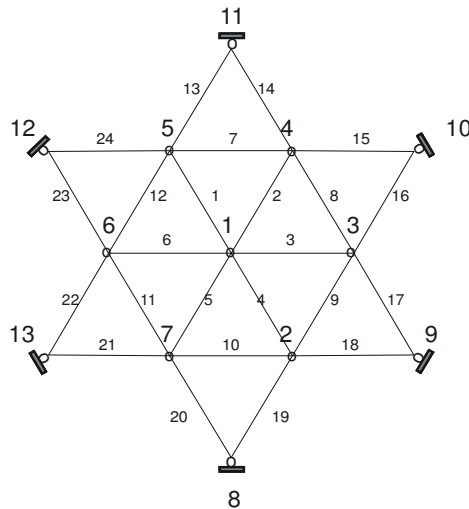


Figure 1. Layout of the 24-member dome structure

Nodal Points	X [m]	Y [m]	Z [m]
1	0.0	0.00	0.000
3	25.0	0.00	2.000
4	12.5	21.65	2.000
10	43.3	25.00	8.216
11	0.0	50.00	8.216

Table 1. Geometry of the 24-member dome structure

The elasticity modulus is $E = 7 \times 10^{10} \text{N/m}^2$. The stress constraints for tension and compression are $25 \times 10^6 \text{N/m}^2$. The density is 27500N/m^3 .

The cross-sectional areas of the truss-members with circular sections are selected from an available catalogue:

$$A_i = \{12.00; 12.25; 12.50; 12.75; 13.00; 13.25; 13.50; 13.75; 15.75\} * 10^{-4} \text{m}^2$$

The applied loads of the 24-member dome structure are $P_1 = 6 \text{kN}$ at the nodal point 1, and $P_{2-7} = 12 \text{kN}$ at the nodal points 2-7, which causes a bifurcation instability phenomenon. The results of the optimization process are shown in Tables 2-4.

Run	Weight	Cross-sections (catalogue values)	Relative error
1	258.506	{12.75,15.75,13.50}	1.408
2	258.013	{12.25,15.50,13.75}	1.215
3	256.994	{13.25,14.25,13.75}	0.815
4	256.940	{13.50,15.25,13.25}	0.794
5	256.549	{12.00,13.50,14.50}	0.641
6	256.447	{13.00,15.00,13.50}	0.601
7	256.440	{12.50,15.50,13.50}	0.598
8	256.440	{12.50,15.50,13.50}	0.598
9	255.953	{12.50,14.75,13.75}	0.407
10	255.953	{12.50,14.75,13.75}	0.407
11	255.950	{12.25,15.00,13.75}	0.406
12	255.899	{12.75,15.75,13.25}	0.386
13	255.463	{12.25,14.25,14.00}	0.215
14	255.409	{12.50,15.25,13.50}	0.193
15	255.406	{12.25,15.50,13.50}	0.192
16	255.406	{12.25,15.50,13.50}	0.192
17	255.402	{12.00,15.75,13.50}	0.191
18	254.916	{12.00,15.00,13.75}	0.000
19	254.916	{12.00,15.00,13.75}	0.000
20	254.916	{12.00,15.00,13.75}	0.000

Table 2. Results of genetic algorithm (GA)

Run	Weight	Cross-sections (catalogue values)	Relative error
1	260.697	{13.75,12.75,14.50}	2.268
2	260.044	{14.25,15.25,13.25}	2.012
3	259.557	{14.25,14.50,13.50}	1.821
4	258.526	{14.25,14.25,13.50}	1.416
5	258.468	{14.25,15.50,13.00}	1.393
6	258.465	{14.00,15.75,13.00}	1.392
7	258.084	{13.25,13.25,14.25}	1.243
8	257.978	{14.00,15.00,13.25}	1.201
9	257.536	{13.00,14.00,14.00}	1.028
10	257.488	{13.75,14.50,13.50}	1.009
11	257.488	{13.75,14.50,13.50}	1.009
12	257.430	{13.75,15.75,13.00}	0.986
13	257.046	{12.75,13.50,14.25}	0.836
14	257.036	{12.00,14.25,14.25}	0.832
15	256.991	{13.00,14.50,13.75}	0.814
16	256.978	{12.00,15.50,13.75}	0.809
17	256.450	{13.25,14.75,13.50}	0.602
18	259.557	{14.25,14.50,13.50}	1.821
19	255.950	{12.25,15.00,13.75}	0.406
20	255.406	{12.25,15.50,13.50}	0.192

Table 3. Results of simulated annealing method (SA)

Run	Weight	Cross-sections (catalogue values)	Relative error
1	264.304	{15.75,12.25,14.25}	3.683
2	263.807	{15.00,12.25,14.50}	3.488
3	262.232	{15.00,12.50,14.25}	2.870
4	262.228	{14.75,12.75,14.25}	2.868
5	262.228	{14.75,12.75,14.25}	2.868
6	260.697	{13.75,12.75,14.50}	2.268
7	260.598	{15.00,14.00,13.50}	2.229
8	260.540	{15.00,15.25,13.00}	2.206
9	259.701	{12.00,13.00,15.00}	1.877
10	259.615	{14.25,13.25,14.00}	1.843
11	259.016	{14.50,14.75,13.25}	1.608
12	259.016	{14.50,14.75,13.25}	1.608
13	258.577	{13.75,13.50,14.00}	1.436
14	258.125	{12.00,13.25,14.75}	1.259
15	258.125	{12.00,13.25,14.75}	1.259
16	258.032	{13.75,14.00,13.75}	1.222
17	256.994	{13.25,14.25,13.75}	0.815
18	256.450	{13.25,14.75,13.50}	0.602
19	255.460	{12.00,14.50,14.00}	0.213
20	254.916	{12.00,15.00,13.75}	0.000

Table 4. Results of tabu search method (TS)

The results obtained using simulated annealing (SA), genetic algorithm (GA), and tabu search (TA) methods have been illustrated in Tables 2-4.

The total number of the cross-sectional combinations for three member groups is 4096. The global optimal solution of the problem: $GW = 254.916$ the weight of the structure; $GC = \{12.00; 15.00; 13.75\}$. Using a standard implicit enumeration algorithm, 1615 node evaluations were needed to obtain this solution and to prove its global optimality. To compare the standard local search methods, we ran each method 20 times from a randomly selected design (population). In each case we stopped the searching process after 150 design evaluations.

4.2. The 10-bar truss. In this comparative study, according to the widely used dimension in the literature we adopted the same values and the same dimension system in our computation.

Load condition: $P = 100000 \text{ lb}$; Material density: $\rho = 0,1 \text{ lb/in}^2$;

Young modulus: $E = 10^7 \text{ psi}$; Yield stress: $\sigma = 40000 \text{ psi} \pm$.

The following conversion table gives us the International System of Units (SI):

1 inch (in) = 25,4 mm ;

1 pound (lb) = 0,4536 kg ;

1 pound per square in (lb/in^2) = 6895 N/m^2 ;

1 $kips$ = 4448 N .

In this example, a genetic algorithm was applied for both cases using One-Point Crossover. The cross-sectional areas are selected from the given set of the catalogue values of $\{ 36; 27; 19; 12; 7; 4; 2; 1 \}$.

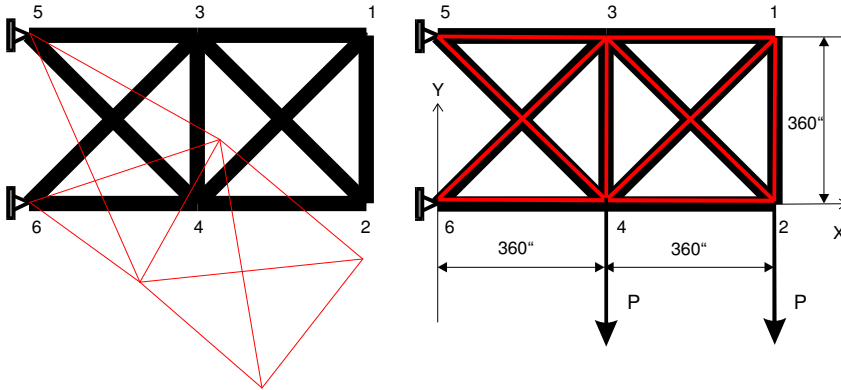


Figure 2. Layout and load condition of the 10-bar truss

The results of the ten-bar truss example (Table 5 and Table 6) demonstrate that the efficiency of GA strongly depends on the choices of population size and the crossover size. Using the nonlinear material law, we obtained much a lighter structure in both cases than in the case of a linear elastic material in the *paper quoted [3]* (see Table 10).

However we have to note that the discrete solution method proposed was different in paper [3].

Population	Crossover	Best weight	Cross-sections
50	50	3028.06	{19,4.,19,2,7,2,7,4,4,7}
50	50	5833.94	{7, 27, 19, 36, 1, 7, 4, 19, 19, 4}
50	50	3819.00	{12, 2, 19, 19, 2, 4, 7, 7, 19, 1}
50	50	3552.09	{19, 4, 19, 7, 2, 1, 2, 12, 12, 7}
50	50	4154.29	{12, 4, 19, 7, 12, 2, 4, 12, 7, 19}
50	50	3727.41	{4, 12, 7, 1, 2, 4, 12, 2, 19, 19}
50	50	3466.23	{12, 27, 19, 7, 2, 1, 4, 7., 7, 2}
50	50	3682.23	{19, 12, 7, 7, 2, 27, 7, 2, 4, 7}
50	50	3725.91	{7, 7, 12, 12, 12, 4, 19, 2, 7, 7}
50	50	4841.91	{7, 12, 19, 4, 7, 36, 12, 19, 2, 2}

Table 5. Results of ten-bar truss

Population	Crossover	Best weight	Cross-sections
100	100	3045.53	{12, 2, 19, 4, 1, 7, 7, 12, 7, 2}
100	100	2823.35	{7, 7, 7, 7, 4, 4, 7, 12, 4, 7}
100	100	4539.00	{7, 7, 19, 7, 2, 36, 7, 1, 7, 19}
100	100	3343.32	{12, 12, 19, 4, 12, 7, 12, 1, 4, 2}
100	100	3708.44	{36, 4, 7, 12, 2, 1, 4, 12, 12, 1}
100	100	3930.62	{7, 7, 19, 27, 7, 4, 12, 4, 7, 4}
100	100	3750.62	{27, 1, 12, 12, 12, 2, 7, 4, 4, 12}
100	100	3908.47	{12, 4, 19, 4, 1, 12, 27, 2, 4, 7}
100	100	4588.41	{4, 19, 27, 12, 36, 4, 12, 1, 1, 4}
100	100	3157.15	{4, 2, 12, 2, 2, 36, 12, 4, 1, 4}

Table 6. Results for ten-bar truss

4.3. **The 25-bar truss.** Material density, Young modulus, and yield stress constraints are the same as for the ten-bar truss. The loads are given in Table 7. The relationship between the indices and the cross-sections is given in Table 8. The results obtained by using the nonlinear material law (see Table 9) are approximately half of the optimal weight obtained using the linear elastic material law (see Table 10).

In this example a genetic algorithm was also applied. The cross-sectional areas are selected from the given set of the catalogue values of

$$\{ 3,5 \ 3,4 \ 3,3 \ \dots \ 1,0 \ 0,9 \ \dots \ 0,2 \ 0,1 \ 0,01 \} .$$

Nodal points	X [kips]	Y [kips]	Z [kips]
1	-	20	-5
2	-	-20	5

Table 7. Applied loads of 25-bar truss

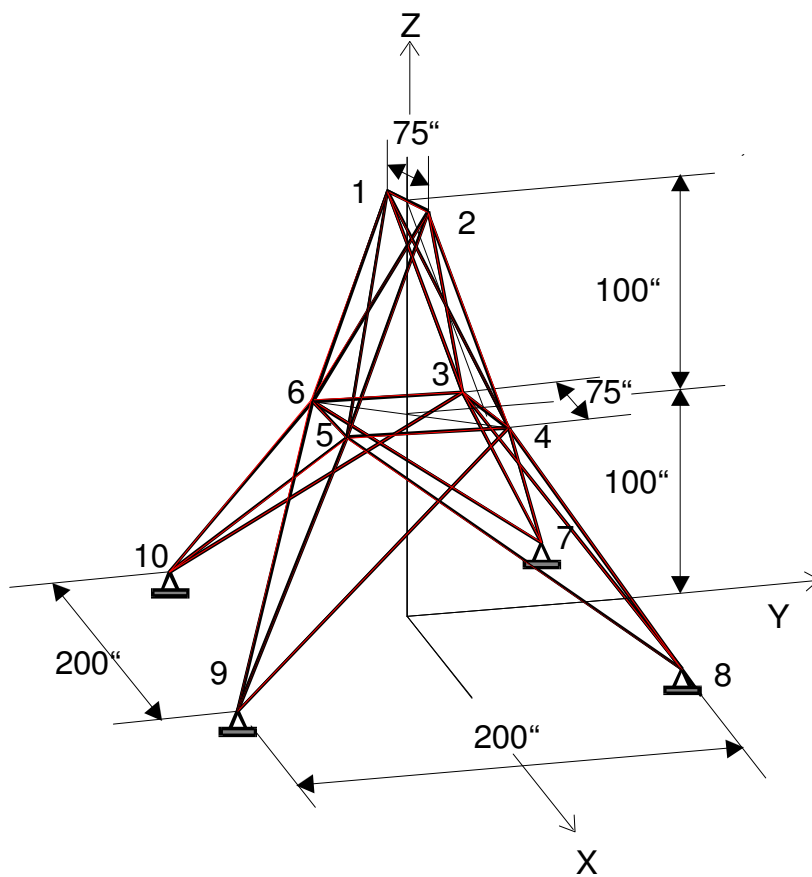


Figure 3. Geometry of the 25-bar truss

[1]=0.01	[2]= 0.1	[3]= 0.2	[4]= 0.3	[5]= 0.4	[6]= 0.5
[7]= 0.6	[8]= 0.7	[9]= 0.8	[10]= 0.9	[11]= 1.0	[12]= 1.1
[13]= 1.2	[14]= 1.3	[15]= 1.4	[16]= 1.5	[17]= 1.6	[18]= 1.7
[19]= 1.8	[20]= 1.9	[21]= 2.0	[22]= 2.1	[23]= 2.2	[24]= 2.3
[25]= 2.4	[26]= 2.5	[27]= 2.6	[28]= 2.7	[29]= 2.8	[30]= 2.9
[31]= 3.0	[32]= 3.1	[33]= 3.2	[34]= 3.3	[35]= 3.4	[36]= 3.5

Table 8. Relationship between the indices and cross-sections

Population	Crossover	Best weight	Cross-sections
50	50	201.678	{12, 5, 3, 14, 17, 5, 7, 10}
50	50	165.837	{3, 6, 12, 15, 13, 3, 4, 4}
50	50	204.183	{10, 11, 16, 3, 17, 3, 5, 3}
50	50	260.231	{15, 15, 10, 8, 3, 6, 11, 4}
50	50	188.972	{30, 8, 9, 5, 11, 5, 3, 7}
50	50	153.736	{27, 4, 4, 12, 15, 3, 4, 7}
50	50	166.926	{13, 3, 6, 6, 15, 5, 9, 3}
50	50	228.348	{8, 4, 13, 23, 16, 3, 7, 9}
50	50	160.656	{27, 4, 9, 3, 7, 3, 7, 5}
50	50	157.644	{15, 6, 4, 7, 13, 6, 5, 4}

Table 9. Results of 25-bar truss

Results of ten-bar truss			Results of twenty-five-bar truss		
Variables	Continuous solution	Discrete method	Variables	Continuous solution	Discrete method
1	30.4015	36.0	1	0.3	0.3
2	0.1	0.1	2	2.03572	2.00
3	23.1041	27.0	3	2.75761	2.80
4	15.2160	19.0	4	0.01	0.01
5	0.1	0.5	5	0.01778	0.01
6	0.6623	0.1	6	0.33511	0.40
7	7.5049	7.0	7	1.9	1.90
8	20.9631	19.0	8	0.1	0.20
9	21.5409	19.0			
10	0.1	0.1			
weight [lb]	5056.15	5273.32		394.027	403.897

Table 10. The optimum cross-sectional areas [in^2] using linear elastic material law

The optimal weight of the 25-bar truss structure is $153.736 lb$ using the nonlinear material law instead of the linear elastic rod members resulting in $403.897 lb$ for discrete design variables and resulting in $394.027 lb$ in the case of continuous solution methods.

5. Conclusions

In this work, three different solution techniques are discussed and compared, simulated annealing (SA), genetic algorithm (GA), and tabu search (TS) methods, for solving a discrete minimal weight design problem for shallow space trusses. In each case we stopped the searching process after 150 design evaluations. The computational results reveal the fact that the GA method produces high quality results when the solution time is limited. Obviously, the performance of SA, TA, and GA depends on various parameter choices, such as the cooling parameter for SA, and the population

size, frequency of mutation for GA. The TA and the SA methods are very sensitive to the starting (initial) design. When the solution time is limited, the likelihood that the TA and SA methods provide near optimal solutions is very low.

We compared the numerical results of two frequently used test problems obtained by using the linear and nonlinear material law. We obtained much lighter structure in both cases but we have to note that the solution method was different in the quoted paper [3] (see Table 7) and in the present study. In contradiction with paper [3], here nodal displacement constraints were not considered. However, the large deflection in the behavior of the initial structure might be significant. In the last two examples, a genetic algorithm (GA) was adopted for the discrete optimal design problem. In each case we stopped the searching process after 150 (300) design evaluations related to a population size of 50 (100).

References

1. ARORA, J. S., HUANG, M. W. and HSICH C. C.: Methods for optimization of nonlinear problems with discrete variables: a review. *Structural Optimization*, **8**, (1994), 69-85.
2. CSÉBFALVI, A.: A non-linear path-following method for computing the equilibrium curve of structures. *Annals of Operation Research* **81**, (1998), 15-23.
3. CSÉBFALVI A. and CSÉBFALVI, G.: A new discrete optimization procedure for geometrically non-linear space trusses, in: Proceedings of Third World Congress of Structural and Multidisciplinary Optimization (WCSMO-3), May 17-21, 1999, Buffalo, New York, 1, 1999, On-line publication:
<http://www.eng.buffalo.edu/Research/MODEL/wcsmo3/proceedings/30SMD/30SMD6.pdf>
4. CSÉBFALVI, A.: Discrete optimal weight design of geometrically nonlinear truss-structures. *Computer Assisted Mechanics and Engineering Sciences*, **6**, (1999), 313-320.
5. CSÉBFALVI, A.: Discrete optimization of shallow trusses with stability constraints, in: Proceedings of the Third International Conference on Coupled Instabilities in Metal Structures (CIMS'2000), eds. D. Camotim, D. Dubina, J. Rondal, September 21-23, 2000, Lisbon, Portugal, Imperial College Press, 635-642, 2000.
6. CSÉBFALVI, A.: A simulated annealing algorithm for discrete minimal weight design of shallow space trusses with stability constraints, WCCM-V Fifth World Congress on Computational Mechanics, July 7-12, 2002, Vienna, Austria, eds. H. A. Mang, F. G. Rammerstorfer, J. Eberhardsteiner, On-line publication (ISBN 3 9501554-0-6) Paper-ID: 81234, Session: RS 207.4, 2002.
7. CSÉBFALVI, A.: Optimal Design of Space Structures with Stability Constraints, in: System-based Vision for Strategic and Creative Design, ed. Bontempi, Swets & Zeitlinger, Lisse, ISBN 90 5809 599 1, 493-497, 2003.
8. GOLDBERG, D. E. and SAMTANI, M. P.: Engineering Optimization via Genetic Algorithms, 9th Conference on Electronic Computation, ASCE, New York, 471-482, 1986.
9. JOHN, K. V. and RAMAKRISHNAN C. V.: Optimum design of trusses from available section - use of sequential linear programming with branch and bound algorithm. *Engineering Optimization*, **13**, (1988), 119-145.
10. KIRKPATRIK, S., GELATT, C. and VECCHI, M.: Optimization by simulated annealing. *Science*, 220, (1983), 671-680.

11. LEITE, J. P. B. and TOPPING, B. H. V.: Parallel simulated annealing for structural optimization. *Computers & Structures*, **73**, (1999), 545-564.
12. RAJEEV, S. and KRISHNAMOORTY C. S.: Discrete optimization of structures using genetic algorithms. *Journal of Structural Engineering ASCE*, **118**(5), (1992), 1233-1250.
13. SALAJEGHEH, E. and SALAJEGHEH, J.: Optimum design of structures with discrete variables using higher order approximation. *Computer Methods in Applied Mechanics and Engineering*. **191**, (2002), 1395-1419.

A RECIPROCAL THEOREM FOR STEADY-STATE HEAT CONDUCTION PROBLEMS

ISTVÁN ECSEDI AND KORNÉL DLUHI
Department of Mechanics, University of Miskolc
3515 Miskolc-Egyetemváros, Hungary
mechecs@uni-miskolc.hu, mechdk@uni-miskolc.hu

[Received: October 8, 2004]

Dedicated to István Páczelt on the occasion of his 65th birthday

Abstract. This paper presents a reciprocal theorem for steady-state heat conduction problems. Some examples illustrate the applications of the reciprocal relation formulated. The method applied is based on the analogy which exists between linear elasticity and heat conduction.

Mathematical Subject Classification: 80A20

Keywords: heat conduction, reciprocal theorem, steady-state, thermal energy

1. Introduction

Consider a 3D solid body B occupying a closed and limited region \bar{V} for which the steady-state heat condition is defined. The set of inner points V is denoted by V and the set of points on the boundary of \bar{V} is denoted by ∂V , $\bar{V} = V \cup \partial V$. Point P of \bar{V} is indicated by the vector $\vec{OP} = \mathbf{p} = x\mathbf{e}_x + y\mathbf{e}_y + z\mathbf{e}_z$ in a given orthogonal Cartesian coordinate system $Oxyz$ with the unit vectors \mathbf{e}_x , \mathbf{e}_y , \mathbf{e}_z . The volume element in V is denoted by dv and the surface element defined on ∂V is da .

The temperature difference field [7, 1] in the body \bar{V} is denoted by $T = T(x, y, z)$. Following Wojnar [7] and the thermal intensity vector field is introduced by the definition

$$\mathbf{t} = -\nabla T, \quad (1)$$

where

$$\nabla = \frac{\partial}{\partial x}\mathbf{e}_x + \frac{\partial}{\partial y}\mathbf{e}_y + \frac{\partial}{\partial z}\mathbf{e}_z \quad (2)$$

is the gradient operator [4, 5]. The field equations of the steady-state heat conduction problem are the heat balance equation [1, 6]

$$-\nabla \cdot \mathbf{q} + R = 0, \quad \text{in } V \quad (3)$$

and the Fourier law of heat conduction [6, 7], which takes the form

$$\mathbf{q} = \mathbf{K} \cdot \mathbf{t}, \quad (4)$$

and the thermal intensity vector–temperature difference field relation (1). In equations (3), (4) the dot denotes the scalar product according to Malvern [5] and Lurje [4]

and in equation (4) $\mathbf{K} = \mathbf{K}(x, y, z)$ is the heat conductivity tensor field, which is symmetric and positive definit [1, 7]. The distributed heat source in B is denoted by $R = R(x, y, z)$. On the boundary surface ∂V the heat flux q is defined at every regular points of ∂V as

$$q = \mathbf{q}(x, y, z) \cdot \mathbf{n} \quad (x, y, z) \in \partial V, \quad (5)$$

where \mathbf{n} is the outward unit normal vector to ∂B at point (x, y, z) .

We say that an ordered array $s = [T, \mathbf{t}, \mathbf{q}]$ is an admissible state if T , \mathbf{t} and \mathbf{q} are sufficiently smooth in \bar{V} and they satisfy equations (1) and (4). The admissible state corresponds to internal heat source R and boundary surface heat flux q if equations (3) and (5) are satisfied. The ordered array of R and q is denoted by p as $p = [R, q]$.

2. Reciprocal theorem

Theorem 1. *Let $s = [T, \mathbf{t}, \mathbf{q}]$ and $\tilde{s} = [\tilde{T}, \tilde{\mathbf{t}}, \tilde{\mathbf{q}}]$ be two admissible states of the stationary heat conduction in body B corresponding to the internal heat sources and surface heat fluxes $p = [R, q]$ and $\tilde{p} = [\tilde{R}, \tilde{q}]$, respectively, then we have*

$$\begin{aligned} \int_V \mathbf{t} \cdot \tilde{\mathbf{q}} \, dv &= \int_V \tilde{\mathbf{t}} \cdot \mathbf{q} \, dv \\ &= - \int_{\partial V} T \tilde{q} \, da + \int_V T \tilde{R} \, dv = - \int_{\partial V} \tilde{T} q \, da + \int_V \tilde{T} R \, dv. \end{aligned} \quad (6)$$

Proof. The validity of equation (6) follows from the equations

$$\begin{aligned} \int_V \mathbf{t} \cdot \tilde{\mathbf{q}} \, dv &= \int_V \mathbf{t} \cdot \mathbf{K} \cdot \tilde{\mathbf{t}} \, dv, \quad \int_V \tilde{\mathbf{t}} \cdot \mathbf{q} \, dv = \int_V \tilde{\mathbf{t}} \cdot \mathbf{K} \cdot \mathbf{t} \, dv, \\ \int_V \tilde{\mathbf{t}} \cdot \mathbf{K} \cdot \mathbf{t} \, dv &= \int_V \mathbf{t} \cdot \mathbf{K} \cdot \tilde{\mathbf{t}} \, dv, \end{aligned} \quad (7)$$

$$\begin{aligned} \int_V \tilde{\mathbf{t}} \cdot \mathbf{K} \cdot \mathbf{t} \, dv &= \int_V \tilde{\mathbf{q}} \cdot \mathbf{t} \, dv = - \int_V \tilde{\mathbf{q}} \cdot \nabla T \, dv = \\ &= - \int_V \nabla \cdot (\tilde{\mathbf{q}} T) \, dv + \int_V T \nabla \cdot \tilde{\mathbf{q}} \, dv = - \int_{\partial V} \mathbf{n} \cdot \tilde{\mathbf{q}} T \, da + \int_V T \tilde{R} \, dv = \\ &= - \int_{\partial V} T \tilde{q} \, dv + \int_V T \tilde{R} \, dv. \end{aligned} \quad (8)$$

Here, the rule for derivation of a product function and the divergence theorem have been used. \square

3. Energy theorems

In [7], Wojnar introduced the thermal energy U corresponding to a continuous thermal intensity field \mathbf{t} defined on \bar{V} by

$$U\{\mathbf{t}\} = \frac{1}{2} \int_V \mathbf{t} \cdot \mathbf{K} \cdot \mathbf{t} \, dv. \quad (9)$$

Theorem 2. Let $s = [T, \mathbf{t}, \mathbf{q}]$ and $\tilde{s} = [\tilde{T}, \tilde{\mathbf{t}}, \tilde{\mathbf{q}}]$ be admissible states corresponding to internal heat sources and boundary surface heat fluxes $p = [R, q]$ and $\tilde{p} = [\tilde{R}, \tilde{q}]$, respectively. Then

$$U\{\mathbf{t}\} \leq U\{\tilde{\mathbf{t}}\} \tag{10}$$

provided

$$-\int_{\partial V} T(\tilde{q} - q) \, da + \int_V T(\tilde{R} - R) \, dv \geq 0, \tag{11}$$

or

$$-\int_{\partial V} q(\tilde{T} - T) \, da + \int_V R(\tilde{T} - T) \, dv \geq 0. \tag{12}$$

Thus, if ∂V_1 and ∂V_2 are complementary surface segments of ∂V ($\partial V = \partial V_1 \cup \partial V_2$, $\partial V_1 \cap \partial V_2 = \{\emptyset\}$), then we have

$$\left. \begin{array}{l} T = \tilde{T} \quad \text{on} \quad \partial V_1 \\ q = 0 \quad \text{on} \quad \partial V_2 \\ R = 0 \quad \text{in} \quad V \end{array} \right\} \Rightarrow U\{\mathbf{t}\} \leq U\{\tilde{\mathbf{t}}\}, \tag{13}$$

or

$$\left. \begin{array}{l} T = 0 \quad \text{on} \quad \partial V_1 \\ q = \tilde{q} \quad \text{on} \quad \partial V_2 \\ R = \tilde{R} \quad \text{in} \quad V \end{array} \right\} \Rightarrow U\{\mathbf{t}\} \leq U\{\tilde{\mathbf{t}}\}. \tag{14}$$

Proof. From the definition of thermal energy U it follows that

$$U\{\tilde{\mathbf{t}}\} = U\{\mathbf{t} + (\tilde{\mathbf{t}} - \mathbf{t})\} = U\{\mathbf{t}\} + U\{\tilde{\mathbf{t}} - \mathbf{t}\} + \int_V \mathbf{t} \cdot \mathbf{K} \cdot (\tilde{\mathbf{t}} - \mathbf{t}) \, dv. \tag{15}$$

On the other hand the application of Theorem 1 to the admissible states $s = [T, \mathbf{t}, \mathbf{q}]$ and $\hat{s} = [\hat{T} = T - \tilde{T}, \hat{\mathbf{t}} = \mathbf{t} - \tilde{\mathbf{t}}, \hat{\mathbf{q}} = \mathbf{q} - \tilde{\mathbf{q}}]$ were $\hat{p} = [\hat{R} = R - \tilde{R}, \hat{q} = q - \tilde{q}]$ yields

$$\begin{aligned} \int_V \mathbf{t} \cdot \mathbf{K} \cdot (\tilde{\mathbf{t}} - \mathbf{t}) \, dv &= -\int_{\partial V} T(\tilde{q} - q) \, da + \int_V T(R - \tilde{R}) \, dv \\ &= -\int_{\partial V} q(\tilde{T} - T) \, da + \int_V R(\tilde{T} - T) \, dv. \end{aligned} \tag{16}$$

We have

$$U\{\tilde{\mathbf{t}} - \mathbf{t}\} \geq 0, \tag{17}$$

since \mathbf{K} is a positive definite symmetric tensor field. From equations (15), (16) and inequality relation (17) we immediately obtain the statements formulated in Theorem 2. \square

Theorem 3. *If the admissible states $s = [T, \mathbf{t}, q]$ and $\tilde{s} = [\tilde{T}, \tilde{\mathbf{t}}, \tilde{q}]$ corresponding to $p = [R, q]$ and $\tilde{p} = [\tilde{R}, \tilde{q}]$ satisfy the following conditions*

$$R = \tilde{R} \qquad \text{in } V, \qquad (18)$$

$$T = \text{arbitrary constant} \qquad \text{on } \partial V_1, \qquad (19)$$

$$q = \tilde{q} \qquad \text{on } \partial V_2, \qquad (20)$$

where ∂V_1 and ∂V_2 are complementary surface segments of ∂V such that $\partial V = \partial V_1 \cup \partial V_2$ and $\partial V_1 \cap \partial V_2 = \{\emptyset\}$, then

$$U\{\mathbf{t}\} \leq U\{\tilde{\mathbf{t}}\}. \qquad (21)$$

Proof. We have, according to the global heat balance equation,

$$\int_{\partial V_1} q \, da = \int_V R \, dv - \int_{\partial V_2} q \, da, \qquad \int_{\partial V_1} \tilde{q} \, da = \int_V \tilde{R} \, dv - \int_{\partial V_2} q \, da. \qquad (22)$$

From equations (18), (20) and (22) it follows that

$$\int_{\partial V_1} (\tilde{q} - q) \, da = 0. \qquad (23)$$

By the use of equations (20) and (23) we can write

$$\int_{\partial V} T(\tilde{q} - q) \, da = T \int_{\partial V_1} (\tilde{q} - q) \, da + \int_{\partial V_2} T(\tilde{q} - q) \, da = 0. \qquad (24)$$

Substitution of equations (20) and (24) into relation (11) we obtain that the statement formulated in Theorem 3 is a direct consequence of Theorem 2. \square

4. Mean heat flux vector

We define the mean heat flux vector $\langle \mathbf{q} \rangle$ corresponding to an admissible state $s = [T, \mathbf{t}, \mathbf{q}]$ and $p = [R, q]$ as

$$\langle \mathbf{q} \rangle = \frac{1}{V} \int_V \mathbf{q} \, dv. \qquad (25)$$

Theorem 4. *The mean heat flux vector of the admissible state corresponding to internal heat source field R and surface heat flux q can be expressed as*

$$\langle \mathbf{q} \rangle = \frac{1}{V} \left(\int_{\partial V} \mathbf{p}q \, da - \int_V \mathbf{p}R \, dv \right). \qquad (26)$$

Proof. Be

$$\tilde{T} = \boldsymbol{\alpha} \cdot \mathbf{p} \qquad (27)$$

in equation (6) where $\boldsymbol{\alpha}$ is a constant vector. A simple computation gives

$$\tilde{R} = -\nabla \cdot \mathbf{K} \cdot \boldsymbol{\alpha} \qquad \text{in } V, \qquad (28)$$

$$\tilde{q} = -\mathbf{n} \cdot \mathbf{K} \cdot \boldsymbol{\alpha} \qquad \text{on } \partial V, \qquad (29)$$

$$\int_{\partial V} \tilde{T}q \, da - \int_V \tilde{T}R \, dv = \boldsymbol{\alpha} \cdot \left(\int_{\partial V} \mathbf{p}q \, da - \int_V \mathbf{p}R \, dv \right), \qquad (30)$$

$$\begin{aligned} \int_{\partial V} T\tilde{q} \, da - \int_V T\tilde{R} \, dv &= - \int_{\partial V} T\mathbf{n} \cdot \mathbf{K} \cdot \boldsymbol{\alpha} \, da + \int_V T\nabla \cdot \mathbf{K} \cdot \boldsymbol{\alpha} \, dv \\ &= - \int_{\partial V} T\mathbf{n} \cdot \mathbf{K} \cdot \boldsymbol{\alpha} \, da + \int_{\partial V} T\mathbf{n} \cdot \mathbf{K} \cdot \boldsymbol{\alpha} \, dv + \int_V \boldsymbol{\alpha} \cdot \mathbf{K} \cdot \mathbf{t} \, dv \\ &= \boldsymbol{\alpha} \cdot \int_V \mathbf{q} \, dv . \end{aligned} \tag{31}$$

In the derivation of equation (31) we have used the rule of differentiation of product function, divergence theorem and equation (4). Combination of equation (30) with equation (31) gives the formula of mean heat flux vector.

We note that formula (26) can be derived only by the use of equations (3) and (5). It is not necessary for $\mathbf{q} = \mathbf{q}(x, y, z)$ in (26) to be the solution of a heat conductance problem [2]. If $\mathbf{q} = \mathbf{q}(x, y, z)$ is a solution of a steady-state heat conduction problem, then it satisfies

$$\nabla \times \mathbf{R} \cdot \mathbf{q} = \mathbf{0} \qquad \text{in } V \tag{32}$$

where \mathbf{R} is the inverse tensor of \mathbf{K} (the thermal resistivity tensor [7, 1] $\mathbf{R} \cdot \mathbf{K} = \mathbf{1}$, $\mathbf{1}$ is the unit tensor). The cross between two vectors in equation (32) denotes their vectorial product according to Lurje [4] and Malvern [5]. Compatibility conditions for \mathbf{q} given by (32) are obtained from equations (1), (4). \square

5. Heat conduction on non-homogeneous curved beam

Consider a curved beam (Figure 1) which is an incomplete torus in the 3D space. A torus-like body is generated by the rotation of a plane figure about axis z whose inner and boundary points are taken from the sets A and ∂A , respectively. The domain $\bar{A} = A \cup \partial A$ is bounded and called the cross-section of curved beam. The curved beam occupies the region $\bar{V} = V \cup \partial V$; $V = \{(r, \varphi, z) | (r, z) \in A, 0 < \varphi < \alpha\}$, $\partial V = A_1 \cup A_2 \cup A_3$, $A_i = \{(r, \varphi, z) | (r, z) \in A \quad \varphi = \varphi_i \quad (i = 1, 2) \quad \varphi_1 = 0, \varphi_2 = \alpha\}$, $A_3 = \{(r, \varphi, z) | (r, z) \in \partial A \quad 0 \leq \varphi \leq \alpha\}$, which is referred to a given cylindrical coordinate system $Or\varphi z$. Unit vectors of the cylindrical coordinate system $Or\varphi z$ are $\mathbf{e}_r = \mathbf{e}_x \cos \varphi + \mathbf{e}_y \sin \varphi$, $\mathbf{e}_\varphi = \mathbf{e}_z \times \mathbf{e}_r$ and \mathbf{e}_z . The polar coordinates r and φ are defined as $r = \sqrt{x^2 + y^2}$, $\tan \varphi = y/x$. The incomplete torus-like body (curved beam) is isotropic and φ -homogeneous. This means that

$$\mathbf{K} = k(r, z) \mathbf{1} , \tag{33}$$

where $k = k(r, z)$ is the thermal conductivity of curved beam (incomplete torus, $0 < \alpha < 2\pi$), which may depend upon the cross-sectional coordinates r and z . The following boundary-value problem of the steady-state heat conduction is analysed:

$$T(r, 0, z) = \vartheta_1(r, z) \qquad \text{on } A_1 \qquad (\vartheta_1(r, z) \text{ is given function on } A_1) , \tag{34}$$

$$T(r, \alpha, z) = \vartheta_2(r, z) \qquad \text{on } A_2 \qquad (\vartheta_2(r, z) \text{ is given function on } A_2) , \tag{35}$$

$$\mathbf{q} \cdot \mathbf{n} = q_3(r, \varphi, z) \qquad \text{on } A_3 \qquad (q_3(r, \varphi, z) \text{ is given function on } A_3) , \tag{36}$$

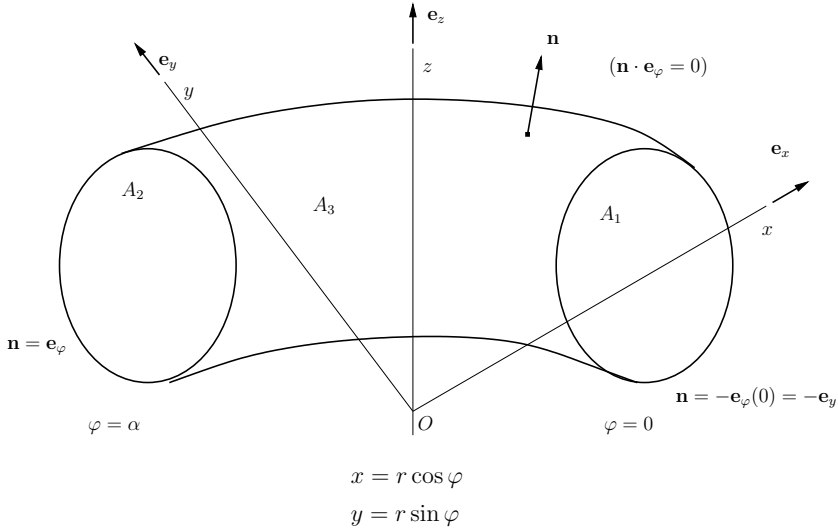


Figure 1. Incomplete non-homogeneous torus (curved beam)

furthermore $R = R(r, \varphi, z)$ is specified in V . Our aim is to obtain the values of heat flux resultants Q_1 and Q_2 which are defined as

$$Q_1 = \int_{A_1} \mathbf{q} \cdot \mathbf{n}_1 \, da = - \int_{A_1} \mathbf{q} \cdot \mathbf{e}_\varphi \, da, \quad (37)$$

$$Q_2 = \int_{A_2} \mathbf{q} \cdot \mathbf{n}_2 \, da = \int_{A_2} \mathbf{q} \cdot \mathbf{e}_\varphi \, da. \quad (38)$$

Here, we note (Figure 1) $\mathbf{n} = \mathbf{n}_1 = -\mathbf{e}_\varphi$ on A_1 , $\mathbf{n} = \mathbf{n}_2 = \mathbf{e}_\varphi$ on A_2 and $\mathbf{n} = \mathbf{n}_3$ on A_3 , $\mathbf{n}_3 \cdot \mathbf{e}_\varphi = 0$. The global heat balance equation for the incomplete torus is formulated as

$$Q_1 + Q_2 + Q_3 - Q_v = 0, \quad (39)$$

where

$$Q_3 = \int_{A_3} q_3 \, da = \int_0^\alpha \left(\oint_{\partial A} r q_3 \, d\sigma \right) d\varphi, \quad (40)$$

$$Q_v = \int_0^\alpha \left(\int_A r R \, dA \right) d\varphi. \quad (41)$$

In equation (40), σ is the arc-length defined on the boundary curve of A . The first equation, which we will use to determine the heat flux resultants Q_1 and Q_2 , is equation (39) and the second one will be derived from the reciprocal relation (6). Let the state $s = [T, \mathbf{t}, \mathbf{q}]$ be the solution of the heat conduction problem of the curved beam specified by boundary conditions (34), (35), (36) with the prescribed internal heat source $R = R(r, \varphi, z)$. The second state of steady heat conduction for the curved

beam shown in Figure 1 is given by the following equations

$$\begin{aligned} \tilde{T} &= C\varphi, & \tilde{\mathbf{t}} &= -\frac{C}{r}\mathbf{e}_\varphi, & \tilde{\mathbf{q}} &= -C\frac{\lambda(r,z)}{r}\mathbf{e}_\varphi, \\ \tilde{R} &= \nabla \cdot \tilde{\mathbf{q}} = 0, & \tilde{q} &= -C\frac{\lambda(r,z)}{r}\mathbf{e}_\varphi \cdot \mathbf{n} & \text{on } A &= A_1 \cup A_2 \cup A_3, \end{aligned}$$

where C is a constant different from zero. It is very easy to show that

$$\int_{\partial V} \tilde{T}q \, da - \int_V \tilde{T}R \, dV = C(I_1 - I_2 + \alpha Q_2), \tag{42}$$

$$\begin{aligned} \int_{\partial V} T\tilde{q} \, da - \int_V T\tilde{R} \, dV \\ = -C \left(\int_{A_2} \frac{\lambda(r,z)}{r} \vartheta_2(r,z) \, da - \int_{A_1} \frac{\lambda(r,z)}{r} \vartheta_1(r,z) \, da \right). \end{aligned} \tag{43}$$

Here,

$$I_1 = \int_{A_3} \varphi q_3 \, da = \int_0^\alpha \oint_{\partial A} r\varphi q_3 \, d\sigma \, d\varphi, \tag{44}$$

$$I_2 = \int_V \varphi R \, dV = \int_0^\alpha \oint_{\partial A} r\varphi R \, da \, d\varphi. \tag{45}$$

Substitution of equations (42) and (43) into reciprocal relation (6) yields

$$Q_2 = -\frac{1}{\alpha} \left(\int_{A_2} \frac{\lambda(r,z)}{r} \vartheta_2(r,z) \, da - \int_{A_1} \frac{\lambda(r,z)}{r} \vartheta_1(r,z) \, da \right) + \frac{I_2 - I_1}{\alpha}. \tag{46}$$

Formula (46) gives the value of heat flux resultant Q_2 without knowing the solution of the corresponding 3D heat conduction problem of the incomplete torus.

6. Mean temperature

Let B be a homogeneous solid sphere. The domain \bar{V} occupied by B is

$$\bar{V} = \{\mathbf{p} = x\mathbf{e}_x + y\mathbf{e}_y + z\mathbf{e}_z \mid p^2 - \varrho^2 \leq 0\},$$

where ϱ is the radius of the bounding spherical surface. The following boundary value problem of heat conduction is considered:

$$R(x, y, z) = R(\mathbf{p}) \quad \text{is prescribed in } V, \tag{47a}$$

$$T(x, y, z) = \vartheta(x, y, z) \quad \text{on } \partial V \quad (\vartheta(x, y, z) \text{ is given function on } \partial V). \tag{47b}$$

It is obvious that equation (47b) formulates a Dirichlet's type boundary condition. The position vector of a point on the spherical surface ∂V is denoted by $\boldsymbol{\varrho}$. Our purpose is to compute the mean value of the temperature field of a solid sphere without knowing the solution of the boundary value problem determined by the prescriptions mentioned above. We use the reciprocal relation (6). The first admissible state is the

solution of the heat conduction problem specified by equations (47a) and (47b). The second admissible state is given by the following equations

$$\tilde{T} = \frac{C}{2}(\varrho^2 - p^2), \quad \tilde{\mathbf{t}} = C\mathbf{p} \quad \text{on } \bar{V}, \quad (48)$$

$$\tilde{\mathbf{q}} = C\mathbf{K} \cdot \mathbf{p} \quad \text{on } \bar{V}, \quad (49)$$

$$\tilde{q} = C k(\varrho) \quad \text{on } \partial V \quad \tilde{R} = CK_I \quad \text{in } V. \quad (50)$$

Here,

$$k(\varrho) = \frac{\varrho \cdot \mathbf{K} \cdot \varrho}{\varrho} \quad \text{defined on } \partial V, \quad K_I = \mathbf{K} \cdot \cdot \mathbf{1}, \quad (51)$$

K_I is the first scalar invariant of the conductivity tensor and the double dot denotes the double dot product of \mathbf{K} and $\mathbf{1}$ according to Malvern [5] and Lurje [4], and we note that \mathbf{K} is constant tensor. Substitution of the fields of two chosen admissible states into formula (6) gives the result

$$\langle T \rangle = \frac{3}{4\pi K_I \varrho^3} \left[\int_{\partial V} k(\varrho) \vartheta(\varrho) \, da + \frac{\varrho^2}{2} \int_V R(\varrho) \, dV - \frac{1}{2} \int_V p^2 R(\mathbf{p}) \, dV \right]. \quad (52)$$

In equation (52) the mean temperature field $\langle T \rangle$ in the sphere is defined as

$$\langle T \rangle = \frac{3}{4\pi \varrho^3} \int_V T(\mathbf{p}) \, dV. \quad (53)$$

7. Conclusions

In this paper, a reciprocal theorem is formulated by the use of the analogy which exists between linear elasticity and heat conduction. The formalism of applied analogy follows Wojnar's approach [7]. The theorems proven are analogous to those obtained in linear elasticity theory by Gurtin [3].

Acknowledgement. The support provided by the Hungarian National Research Foundation within the framework of projects T049115 and T037759 is gratefully acknowledged.

References

- CARLSON, D. E.: Linear thermoelasticity. [in:] S. FLÜGGE [Ed.], *Handbuch der Physik*, Vol. VIa/2, Mechanics of Solids II. 297–345, Springer, Berlin 1972.
- ECSEDI, I.: Mean value and bounding formulae for heat conduction. *Archives of Mechanics*, **54**(2), (2002), 127–140.
- GURTIN, M. E.: The linear theory of elasticity. [in:] S. FLÜGGE [Ed.], *Handbuch der Physik*, Vol. VIa/2, Mechanics of Solids II. pp. 1–295, Springer, Berlin 1972.
- LURJE, A. I.: *Theory of elasticity*. Nauka, Moscow 1970. (in Russian)
- MALVERN, L. E.: *Introduction to the mechanics of a continuous medium*. Prentice-Hall, New York 1969.
- ÖZISIK, M. N.: *Boundary value problems of heat conduction*. Dover Publications, New York 1989.
- WOJNAR, R.: Upper and lower bounds on heat flux. *Journal of Thermal Stresses*, **21**, (1998), 381–403.

ECONOMY OF WELDED STIFFENED STEEL PLATES AND CYLINDRICAL SHELLS

JÓZSEF FARKAS

Department of Materials Handling and Logistics, University of Miskolc
3515 Miskolc-Egyetemváros, Hungary
altfar@uni-miskolc.hu

[Received: April 12, 2004]

Dedicated to István Páczelt on the occasion of his 65th birthday

Abstract. The main requirements for modern load-carrying structures are safety, producibility and economy. Economy is characterized by cost. We have developed a structural optimization system which assures the safety and producibility by fulfillment of design and fabrication constraints, and economy is achieved by minimization of a cost function. Using this system it is possible to make realistic comparisons between different structural versions. This is based on a cost calculation method which is developed mainly for welded structures. The thickness of plates and shells can be decreased by stiffening. Stiffened structures are economic, when the cost difference caused by thickness reduction is higher than the additional cost of stiffening material and welding. It is shown by numerical problems that stiffening is economic only in case when the sensitivity of plates and shells to buckling or transverse deformation can effectively be eliminated by it.

The economy of stiffened structures depends on the type of load and stiffening. Since plates are very sensitive to buckling and transverse deformation, their stiffening is always effective and economic. Cylindrical shells are sensitive to buckling in the case of external pressure thus ring-stiffening is economic in this case. On the other hand, they are not very sensitive to buckling in the case of axial compression or bending, thus ring-stiffening is uneconomic for these loads and stringer-stiffening is economic only in cases when the transverse deformation of the whole shell is limited.

Mathematical Subject Classification: 74K20, 74K25, 74P10

Keywords: stiffened plates and shells, welded structures, buckling, minimum cost design, structural optimization, fabrication cost calculation, economy

1. Introduction

One of the most important characteristics of welded structures is cost for welding is an expensive fabrication process. Cost is a realistic basis for the comparison of different structural versions. Optimization is needed to decrease the cost in order to develop competitive structures.

The most effective method to decrease the structural mass is to decrease thickness. Thin-walled structures show the following problems: large deformations, large residual welding stresses and distortions, buckling, vibration, sensitivity to torsion,

fatigue due to large stress concentrations. To avoid these problems, stiffening can be used. Stiffening enables thickness to be decreased, but it incurs the additional cost of stiffener material and welding. Therefore stiffening is economic only in cases when the cost difference caused by thickness reduction is higher than the additional cost of stiffening material and welding.

In our research we have worked out several minimum mass or cost design problems related to stiffened plates and shells [1]. Our experience is that cost savings due to stiffening are different, in some cases the cost of an unstiffened structure is lower than that of the stiffened one. The aim of the present study is to give an overview of these optimization results.

In order to give realistic comparisons between stiffened and unstiffened structures, both structural versions should be optimized. Since optimization processes are complicated, only numerical treatments are possible. Therefore the conclusions of these comparisons cannot be general. In spite of this disadvantage, the results of this study can be useful for designers in selecting the most suitable structural versions.

The main components of an optimum design process are as follows: design constraints, fabrication aspects, cost function and mathematical algorithms of constrained function minimization. These components affect the comparisons, thus, it is important to use realistic aspects mainly in cost calculation. Therefore we try to formulate the cost function as realistically as possible.

For the design constraints the rules of API [2], ECCS [3] or DNV [4] can be used.

2. A welded stiffened plate subject to uniaxial compression

The plate is stiffened by ribs of three types as follows: flat, L-shape and trapezoidal shapes – see Figure 1. For the buckling stress constraint the Mikami-Niwa formulae [5] are used which consider the effect of residual welding stresses and initial imperfections. The unknowns are the number of stiffeners, thickness of the base plate (t_F) and stiffener dimensions (in the case of trapezoidal stiffeners the thickness is t_3 , Figure 2).

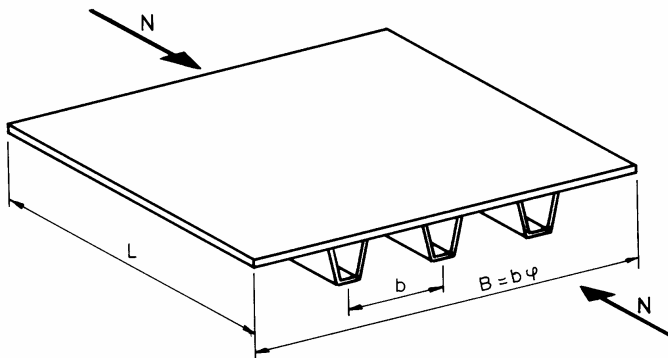


Figure 1. Uniaxially compressed plate with trapezoidal stiffeners

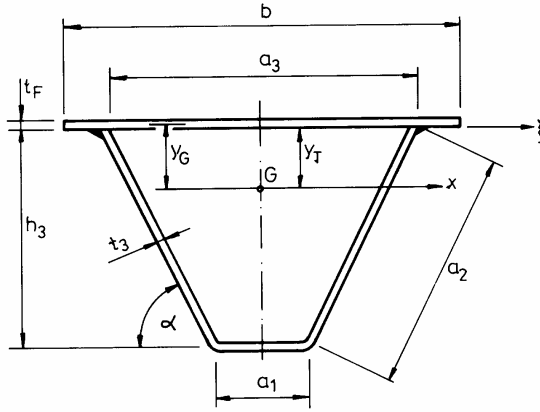


Figure 2. Dimensions of a trapezoidal stiffener

The overall buckling constraint is expressed in function of the reduced slenderness

$$\lambda = (f_y / \sigma_{cr})^{1/2} \tag{1}$$

where σ_{cr} is the classical critical buckling stress, which does not contain the above mentioned effects and, f_y is the yield stress.

The classical critical buckling stress for a uniaxially compressed longitudinally stiffened plate (Figure 1) is

$$\sigma_{cr} = \frac{\pi^2 D}{h B^2} \left(\frac{1 + \gamma_S}{\alpha_R^2} + 2 + \alpha_R^2 \right) \quad \text{for} \quad \alpha_R = L/B < \alpha_{R0} = (1 + \gamma_S)^{1/4} \tag{2}$$

$$\sigma_{cr} = \frac{2\pi^2 D}{h B^2} \left[1 + (1 + \gamma_S)^{1/2} \right] \quad \text{for} \quad \alpha_R \geq \alpha_{R0} \tag{3}$$

where, with

$$\nu = 0.3, \quad D = \frac{E t_F^3}{12(1 - \nu^2)} = \frac{E t_F^3}{10.92} \tag{4}$$

we have

$$h = t_F + \frac{A_S}{b}, \quad b = \frac{B}{\varphi}, \tag{5a}$$

$$A_S = (a_1 + 2a_2) t_3, \quad I_S = a_1 h_3^3 t_3 + \frac{2}{3} a_2^3 t_3 \sin^2 \alpha. \tag{5b}$$

According to the Stahlbau Handbuch [6] $a_1 = 90$, $a_3 = 300$ mm, thus

$$h_3 = (a_2^2 - 105^2)^{1/2}, \quad \sin^2 \alpha = 1 - \left(\frac{105}{a_2} \right)^2. \tag{5c}$$

Here A_S is the cross-sectional area of a stiffener, $\varphi - 1$ is the number of stiffeners,

$$\gamma_S = \frac{E I_S}{b D} \tag{6}$$

and I_S is the moment of inertia of a stiffener about the ξ axis.

Local buckling of a trapezoidal stiffener is defined as

$$a_2/t_3 \leq 38\varepsilon . \quad (7)$$

This constraint is treated as active.

Single panel buckling. This constraint eliminates the local buckling of the base plate parts between the stiffeners. From the classical buckling formula for a simply supported uniformly compressed bar we obtain

$$\sigma_{crP} = \frac{4\pi^2 E}{10.92} \left(\frac{t_F}{b} \right)^2 \quad (8)$$

the reduced slenderness is

$$\lambda_P = \left(\frac{4\pi^2 E}{10.92 f_y} \right)^{1/2} \frac{b}{t_F} = \frac{b/t_F}{56.8\varepsilon} , \quad \varepsilon = \left(\frac{235}{f_y} \right)^{1/2} \quad (9)$$

and the actual local buckling stress considering the initial imperfections and residual welding stresses is

$$\sigma_{UP}/f_y = 1 \quad \text{for } \lambda_P \leq 0.526 , \quad (10a)$$

$$\frac{\sigma_{UP}}{f_y} = \left(\frac{0.526}{\lambda_P} \right)^{0.7} \quad \text{for } \lambda_P \geq 0.526 . \quad (10b)$$

Then the factor ρ_P is as follows:

$$\rho_P = \begin{cases} 1 & \text{if } \sigma_{UP} > \sigma_U , \\ \sigma_{UP}/f_y & \text{if } \sigma_{UP} \leq \sigma_U . \end{cases} \quad (11)$$

Knowing the reduced slenderness (1) the actual global buckling stress can be calculated as follows:

$$\sigma_U/f_y = \begin{cases} 1 & \text{for } \lambda \leq 0.3 , \\ 1 - 0.63(\lambda - 0.3) & \text{for } 0.3 \leq \lambda \leq 1 , \\ 1/(0.8 + \lambda^2) & \text{for } \lambda > 1 . \end{cases} \quad (12)$$

The global buckling constraint is defined by

$$\frac{N}{A} \leq \sigma_U^* = \sigma_U \frac{\rho_P + \delta_S}{1 + \delta_S} \quad (13)$$

where

$$A = Bt_F + (\varphi - 1) A_S \quad (14)$$

and

$$\delta_S = \frac{A_S}{bt_F} . \quad (15)$$

Here ρ_P can be determined considering the single panel buckling of the base plate parts between the stiffeners. The factor $(\rho_P + \delta_S)/(1 + \delta_S)$ expresses the effect of the effective width of the base plate parts.

The cost function is given by

$$\frac{K}{k_m} = \rho V + \frac{k_f}{k_m} \left(\Theta_{dW} \sqrt{\kappa \rho V} + 1.3T_2 \right) , \quad (16)$$

in which V is the structural volume.

For fillet welds using GMAW-M (gas metal arc welding with mixed gas)

$$V = BLt_F + (\varphi - 1) LA_S; \quad \kappa = \varphi; \quad T_2 = 0.3258x10^{-3}a_W^2(\varphi - 1)2L. \quad (17)$$

Here $a_W = 0.5t_3$ but $a_{Wmin} = 4$ mm.

Numerical example. Given data: $B = 6000$ mm, $L = 3000$ mm, $N = 1.974 \times 10^7$ [N], $f_y = 235$ MPa, $E = 2.1 \times 10^5$ MPa, $G = E/2.6$, $\rho = 7.85 \times 10^{-6}$ kg/mm³, $\Theta_{dW} = 3$.

The results of the optimization can be seen in Figure 3. The optimal dimensions are as follows: $t_F = 11$, $t_3 = 8$ mm.

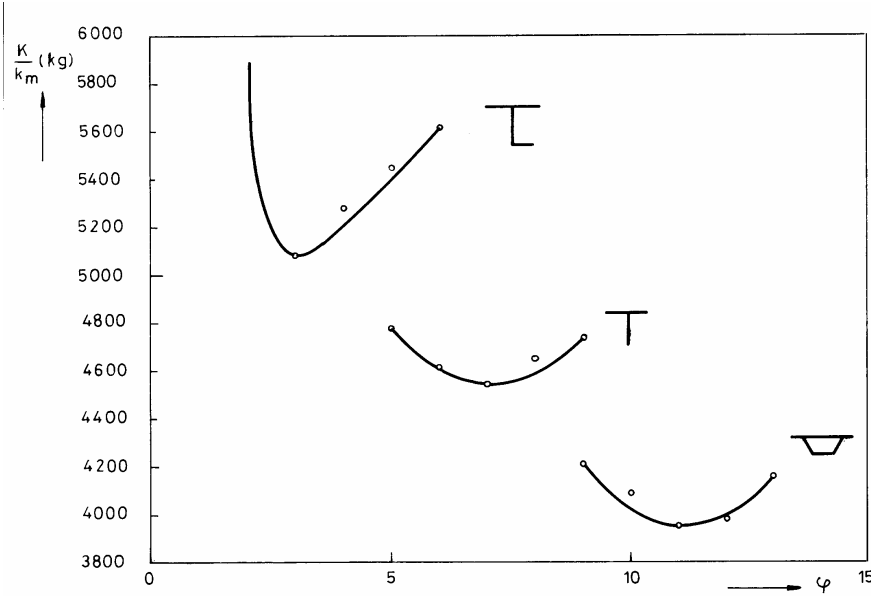


Figure 3. Cost curves in the region of the optimum number of flat, L- and trapezoidal stiffeners for $k_f/k_m = 2$ kg/min

For an unstiffened plate we have

$$\gamma_S = 0, \quad \alpha_{R0} = 1, \quad \alpha_R = 0.5, \quad h = t_F, \quad D = Et_F^3/10.92$$

and

$$\sigma_{cr} = \frac{6.25\pi^2 Et_F^2}{10.92B^2}; \quad \lambda = \frac{84.45}{t_F}. \quad (18)$$

The buckling constraint

$$\frac{N}{A} = \frac{1.974x10^7}{6x10^3 t_F} \leq \sigma_U \quad (19)$$

is fulfilled with $t_F = 51$ mm ($64.5 < 66.4$ MPa).

The cost of the unstiffened plate is

$$\frac{K}{k_m} = \rho BLt_F = 7206 \text{ kg.}$$

It can be seen that the cost of the optimized stiffened plate with trapezoidal ribs (3940 kg) is by 82% cheaper than the unstiffened one. Thus, in this case the economy of the stiffened structural version is evident.

3. An orthogonally stiffened square plate loaded by bending

A square plate with simply supported edges, loaded by uniformly distributed normal load is considered [1, 7]. The plate is stiffened by flat ribs in two directions (Figure 4). The ribs are continuous in one direction, in the other direction they are interrupted and welded to the others by double fillet welds. The size of a fillet weld is $a_W = 0.4t_S$, but $a_{Wmin} = 4\text{mm}$.

Data: $b = 6\text{ m}$, $p_0 = 5 \times 10^{-3}\text{ N/mm}^2$, the yield stress for steel is 235 MPa, the admissible stress is $\sigma_{adm} = 120\text{ MPa}$, the elastic modulus is $E = 2.1 \times 10^5\text{ MPa}$, $\rho = 7.85 \times 10^{-6}\text{ kg/mm}^3$.

In the optimization procedure we search for the optimum values of the following variables: t_F , h , t_S and φ . The number of stiffeners is $\varphi - 1$.

It is assumed that the base plate is welded with butt welds from 4 strips of dimensions $6\text{m} \times 1.5\text{m}$. Then the stiffeners are welded to the base plate by double fillet welds. Finally the interrupted ribs are welded to the other ribs by double fillet welds.

For the butt welds GMAW-M technology is used, thus, the welding time depends on the thickness of the base plate as follows [1]:

$$T_2' = \begin{cases} 3b \times 0.1861 \times 10^{-3} t_F^2 & \text{for } t_F \leq 15\text{ mm} \\ 3b \times 0.1433 \times 10^{-3} t_F^{1.9035} & \text{for } t_F > 15\text{ mm} \end{cases} \quad (20)$$

For longitudinal fillet welds the GMAW-M technology is used, thus, the welding time is

$$T_2'' = 4b(\varphi - 1) \times 0.3258 \times 10^{-3} a_W^2, \quad (21)$$

for transverse fillet welds the SMAW (shielded metal arc welding) technology is assumed, thus

$$T_2''' = 4h(\varphi - 1)^2 \times 0.7889 \times 10^{-3} a_W^2. \quad (22)$$

The volume of the structure is

$$V = b^2 t_F + 2(\varphi - 1) b h t_S. \quad (23)$$

The number of assembled elements is $\kappa = 3 + \varphi^2$. The cost function can be formulated as

$$\frac{K}{k_m} = \rho V + \frac{k_f}{k_m} \left[\Theta_{dW} (\kappa \rho V)^{0.5} + 1.3 (T_2' + T_2'' + T_2''') \right], \quad (24)$$

where $\Theta_{dW} = 3$.

Constraint on compressive stress in the central faceplate element is expressed by

$$\sigma_{\max} = \sigma_{\max.1} + \sigma_{f.\max} \leq \sigma_{adm}. \quad (25)$$

Here $\sigma_{\max.1}$ is caused by the bending of the whole plate, $\sigma_{f.\max}$ is the normal stress due to local bending of the plate elements, σ_{adm} is the admissible stress:

$$\sigma_{\max.1} = \frac{c_M p b^2}{I_x / a} y_G. \quad (26)$$

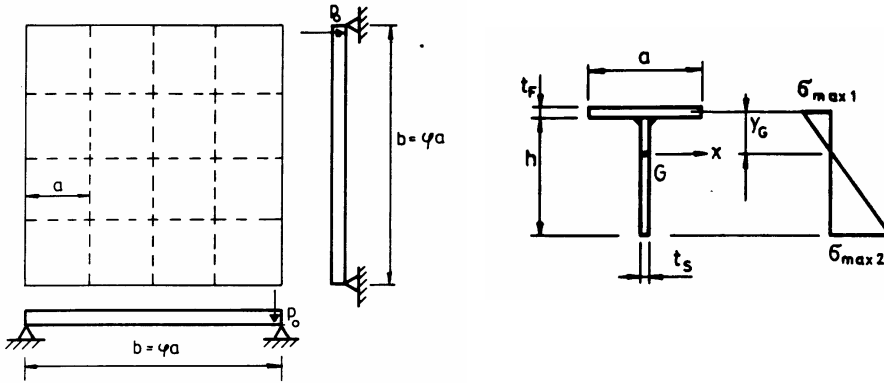


Figure 4. A simply supported transversely uniformly loaded square plate stiffened by flat ribs

The uniformly distributed normal load p contains also the self weight, approximately $p = 1.1p_0$. Since the torsional stiffness of the open section ribs is very small, the stiffened plate can be calculated as an orthotropic one having zero torsional stiffness. Schade [8] calculated for this case $c_M = 0.1102$.

As shown in Figure 4, the distance of the centroidal axis y_G can be calculated as

$$y_G = \frac{h}{2} \frac{1}{1 + \alpha}, \quad \alpha = \frac{at_F}{ht_S} = \frac{bt_F}{\varphi ht_S} \quad (27)$$

and the moment of inertia is

$$I_x = \frac{h^3 t_S}{12} \frac{1 + 4\alpha}{1 + \alpha}. \quad (28)$$

It should be noted that the admissible stress is selected so low that it is not necessary to calculate with an effective width of the face plate, thus $a = b/\varphi$.

The local bending stress can be calculated by means of formulae valid for isotropic square plates with clamped edges (Timoshenko [9])

$$\sigma_{f, \max} = \frac{5.13 \times 10^{-2} p_0 a^2}{t_F^2 / 6} = \frac{0.3078 p_0 b^2}{\varphi^2 t_F^2}. \quad (29)$$

Constraint on the maximum tensile stress in the central ribs can be written as

$$\sigma_{\max, 2} = \sigma_{\max, 1}(1 + 2\alpha) \leq \sigma_{adm}. \quad (30)$$

Constraint on local buckling of the central face plate element compressed from both sides (Farkas & Jármai [10], Volmir [11]). For a plate compressed on one side the buckling factor is $k = 4$. Instead of this value we calculate with $k = 2$. For $k = 4$ Eurocode 3 [12] gives for the limiting slenderness

$$(a/t_F)_{\lim} = 42\varepsilon, \quad \varepsilon = (235/f_y)^{0.5}, \quad (31)$$

f_y is the yield stress, but instead of using the yield stress we can calculate with the maximum stress. Thus, for $k = 2$ the buckling constraint can be written as

$$a/t_F \leq 42\varepsilon_1/\sqrt{2} \approx 30\varepsilon_1, \quad \varepsilon_1 = (235/\sigma_{\max.1})^{0.5}. \quad (32)$$

Constraint on local buckling of ribs (it is assumed that $\sigma_{\max.2}$ can also be compressive)

$$h/t_S \leq 14\varepsilon_2, \quad \varepsilon_2 = (235/\sigma_{\max.2})^{0.5}. \quad (33)$$

Constraint on shear buckling of ribs at the plate edges can be formulated as

$$\tau = \frac{0.42pb^2}{ht_S\varphi} \leq \frac{\tau_{ub}}{\gamma_b} = \frac{5.34\pi^2 E}{12(1-\nu^2)\gamma_b} \left(\frac{t_S}{h}\right)^2 \quad \text{for} \quad \frac{\tau_{ub}}{\gamma_b} \leq \tau_{adm} \quad (34)$$

and

$$\tau \leq \tau_{adm} \quad \text{for} \quad \frac{\tau_{ub}}{\gamma_b} \geq \tau_{adm}. \quad (35)$$

The factor 0.42 is considered, since the distribution of edge reactions is not uniform along the edges (Timoshenko [9]). $\tau_{adm} = \sigma_{adm}/\sqrt{3}$ is the admissible shear stress, ν is the Poisson ratio.

Constraint on residual distortion due to shrinkage of welds is formulated as follows.

Although the stiffeners are welded along two directions, we do not multiply residual deflection by 2. A multiplying factor of 1.5 is used considering the fact that the longitudinal double fillet welds are intermittent due to interruption of ribs and the residual plastic zones of the continuous welds affect the deflection caused by intermittent welds. Thus the distortion constraint is formulated as

$$f = 1.5Cb^2/8 \leq f_{adm}, \quad (36)$$

where the admissible deflection is assumed to be $f_{adm} = b/1000 = 6$ mm.

The orthotropic plate bending theory is valid only in the case when the number of stiffeners is more than 3, thus

$$\varphi \geq 4. \quad (37)$$

It can be seen that the objective function and the design constraints are highly nonlinear. For the constrained function minimization Rosenbrock's hillclimb mathematical programming method is used (a detailed description can be found in Farkas & Jármai [10]) complemented by an additional discretization of the continuous optima considering rounded dimensions and integer numbers of stiffeners.

The optimization results in the following values: for $k_F/k_m = 2$, $t_F = 11$, $h = 250$, $t_S = 14$ mm, $\varphi = 4$ and the corresponding cost is $K/k_m = 9317$ kg. The maximum deflection in the center due to the normal load is

$$w_{\max} = 0.0083 \frac{p_0 b^4}{B_x} = 6.06 < \frac{b}{300} = 20 \text{ mm}, \quad (38)$$

where

$$B_x = \frac{EI_x}{a} = 8.8684 \times 10^9 \text{ Nmm}, \quad I_x = \frac{h^3 t_S}{12} \frac{1 + 4\alpha}{1 + \alpha} = 6.3346 \times 10^7 \text{ mm}^4, \quad (39)$$

$$\alpha = \frac{at_F}{ht_S} = 4.7143.$$

The thickness required for an unstiffened plate to fulfil the deflection constraint of

$$w_{\max} = 0.065 \frac{p_0 b^4}{Et_F^3/10.92} \leq w_{adm} = 20 \text{ mm} \quad (40)$$

is $t_{F0} = 103 \text{ mm}$ and the corresponding cost is $K/k_m = \rho b^2 t_{F0} = 29108 \text{ kg}$.

It can be seen that the stiffened plate which fulfils the stress and deflection constraints is much cheaper (9317 kg) than the unstiffened one (29108 kg). It can be concluded that a plate subject to normal load is very weak against deflection, thus stiffening in this case is also economic.

From the above cases of stiffened plates it can be concluded that their stiffening is economic, since they are very sensitive to buckling as well as to large transverse deformation and stiffening eliminates these sensitivities.

4. A ring-stiffened cylindrical shell subject to external pressure

The design constraints are formulated according to API rules [2].

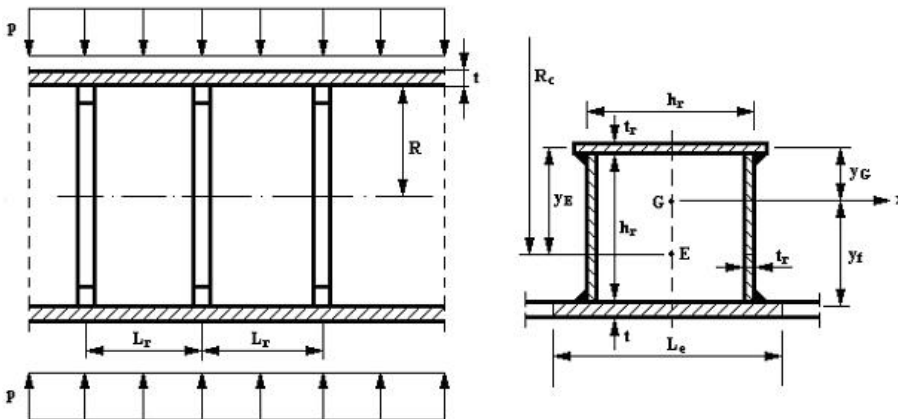


Figure 5. Ring-stiffened cylindrical shell

Geometric characteristics. Data: length of shell $L_b = 15 \text{ m}$, welded from 5 m long segments, radius of shell $R = 1850 \text{ mm}$, intensity of the external pressure $p = 0.5 \text{ MPa}$, yield stress of steel $f_y = 355 \text{ MPa}$. To avoid tilting of the ring-stiffeners, the welded square box section is used, which is characterized by height h_r and thickness t_r . Considering the local buckling constraint of the stiffener flange active, we use the following correlation between height and thickness

$$t_r = \delta_r h_r; \delta_r = 1/42\varepsilon; \varepsilon = \sqrt{235/f_y}; \delta_r = 1/34. \quad (41)$$

The cross-sectional area of a stiffener is

$$A_r = 3h_r t_r = 3\delta_r h_r^2. \quad (42)$$

The distances of centroid G are as follows (Figure 5)

$$y_G = \frac{h_r}{3}, \quad y_r = \frac{2h_r}{3} + \frac{t}{2}, \quad (43)$$

$$y_E = \frac{L_e t (h_r + \frac{t}{2}) + \delta_r h_r^3}{3\delta_r h_r^2 + L_e t}, \quad (44)$$

$$L_e = \begin{cases} 1.1\sqrt{2Rt} & \text{if } M_x = \frac{L_r}{\sqrt{Rt}} > 1.56, \\ L_r & \text{if } M_x \leq 1.56. \end{cases} \quad (45)$$

The distance of the centroid E of the cross-section consisting of the stiffener and the effective part of the shell is characterized by

$$R_C = R - \left(h_r - y_E + \frac{t}{2} \right). \quad (46)$$

The moment of inertia of the stiffener and the effective part of shell is

$$I_{er} = \frac{\delta_r h_r^4}{6} + A_r y_r^2 K_G + \frac{L_e t^2}{12}; \quad K_G = \frac{L_e t}{A_r + L_e t}, \quad (47a)$$

where

$$K_G = \frac{L_e t}{A_r + L_e t}. \quad (47b)$$

Design constraints

Constraint on local shell buckling

$$\gamma_b p \frac{R}{t} \leq \eta_L \sigma_{UL}, \quad (48)$$

where $\gamma_b = 1.5$ is the safety factor and the plasticity reduction factor η_L is calculated in function of $\delta_L = \sigma_{UL}/f_y$ as follows

$$\eta_L = \begin{cases} 1 & \text{if } \delta_L \leq 0.55, \\ \frac{0.45}{\delta_L} + 0.18 & \text{if } 0.55 < \delta_L \leq 1.6, \\ \frac{1.31}{1 + 1.15\delta_L} & \text{if } 1.6 < \delta_L < 6.25, \\ \frac{1}{\delta_L} & \text{if } \delta_L \geq 6.25. \end{cases} \quad (49)$$

The ultimate local buckling strength is

$$\sigma_{UL} = \alpha_L p_{eL} \frac{R}{t} K_L, \quad (50)$$

where $\alpha_L = 0.8$ is the imperfection factor, and for our numerical example $K_L = 1$.

$$p_{eL} = \begin{cases} \frac{1.27E}{A^{1.18} + 0.5} \left(\frac{t}{R}\right)^2 & \text{if } M_x > 1.5 \text{ and } A = M_x - 1.17 < 2.5, \\ \frac{0.92E}{A} \left(\frac{t}{R}\right)^2 & \text{if } 2.5 < A < 0.208Rt, \\ 0.836C_P^{-1.061} E \left(\frac{t}{R}\right)^3 & \text{if } 0.208 < C_P = \frac{A}{R/t} < 2.85, \\ 0.275E \left(\frac{t}{R}\right)^3 & \text{if } C_P > 2.85. \end{cases} \quad (51)$$

Constraint on general shell buckling

$$\gamma_b p \frac{R}{t} \leq \eta_G \sigma_{UG}, \quad (52)$$

where the plasticity reduction factor η_G is calculated in function of $\delta_G = \sigma_{UG}/f_y$ with the same formulae as in the case of η_L – see equation (44):

$$\sigma_{UG} = \frac{\alpha_G}{1.2} p_{eG} \frac{R}{t} K_G. \quad (53)$$

Here $\alpha_G = 0.8$ is the imperfection factor, K_G is defined by equation (42)₂, and a factor of 1.2 is recommended to avoid the mode interaction (coupled instability):

$$p_{eG} = \frac{E \frac{t}{R} \lambda_G^4}{(n^2 - 1)(n^2 + \lambda_G^2)^2} + \frac{EI_{er}(n^2 - 1)}{L_r R_C^2 R}, \quad (54)$$

where

$$\lambda_G = \frac{\pi R}{L_b} = \frac{1850\pi}{15000} = 0.3875,$$

n is the value which gives the minimum value of p_{eG} , $n_{min} = 2$, $n_{max} = 10$. For our case $n = 2$ is used.

The cost function includes the material, fabrication and painting costs:

$$K = K_M + K_F + K_P. \quad (55)$$

The material cost is

$$K_M = k_M \rho V, \quad (56)$$

k_M [\$\$/kg] is the material cost factor and V is the volume of the structure:

$$V = 2\pi R t L_b + n_r \left[4\pi \delta_r h_r^2 \left(R - \frac{h_r}{2} \right) + 2\pi \delta_r h_r^2 (R - h_r) \right], \quad (57)$$

where n_r is the number of ring-stiffeners.

For a fabrication phase it is

$$K_F = k_F \left(\Theta_{dW} \sqrt{\kappa \rho V} + 1.3 C_W a_W^n L_W \right), \quad (58)$$

where k_F (\$\$/min) is the fabrication cost factor, $\Theta_{dW} = 3$ is the difficulty factor expressing the complexity of a structure regarding assembly, the first member calculates time for assembly and tacking, κ is the number of structural parts to be assembled,

the second member calculates the time of welding and additional works (changing the electrode, deslagging, chipping). The additional works are considered by a factor of 1.3. L_W is the weld length, a_W is the weld size, C_W and n are given for different welding technologies and weld type (butt or fillet).

The fabrication cost function is formulated according to the fabrication sequence as follows.

- (1) Welding of a shell segment from 3 parts without stiffeners with GMAW-C butt welds, number of structural parts to be assembled is 3

$$K_{F1} = 3\sqrt{3\rho V_S} + 1.3x0.2245x10^{-3}t^2x3L_S, \quad (59)$$

where $L_S = 3000$ mm, $V_S = 2R\pi tL_S$.

- (2) Welding of a ring-stiffener from 3 plate parts with 2 fillet welds of GMAW-C (gas metal arc welding with CO₂), weld size $a_W = 0.7t_r$

$$K_{F2} = 3\sqrt{3\rho V_r} + 1.3x0.3394x10^{-3}a_W^2x4\pi(R - h_r), \quad (60)$$

where $V_r = 4\pi\delta_r h_r^2 \left(R - \frac{h_r}{2}\right) + 2\pi\delta_r h_r^2 (R - h_r)$.

- (3) Welding of $n_r/5$ stiffeners to a shell segment with 2 fillet welds of size $a_W = 0.7t_r$, GMAW-C

$$K_{F3} = 3\sqrt{\left(\frac{n_r}{5} + 1\right)\rho V_3} + 1.3 \times 0.3394 \times 10^{-3} a_w^2 x 4\pi R n_r / 5, \quad (61)$$

where $V_3 = V_S + V_r n_r / 5$.

- (4) Welding of 5 stiffened shell segments together with butt welds GMAW-C

$$K_{F4} = 3\sqrt{5\rho 5V_3} + 1.3 \times 0.2245 \times 10^{-3} t^2 \times 8R\pi \quad (62)$$

The total material cost is

$$K_M = k_M \rho 5V_3. \quad (63)$$

The total fabrication cost is

$$K_F = k_F (5K_{F1} + n_r K_{F2} + 5K_{F3} + K_{F4}). \quad (64)$$

The painting cost is

$$K_P = k_P \left[2R\pi L_b + 2R\pi (L_b - n_r h_r) + 2\pi (R - h_r) h_r + 4\pi \left(R - \frac{h_r}{2} \right) \right]. \quad (65)$$

In the numerical example the following cost factors are used: $k_M = 1.0$ \$/kg, $k_F = 1.0$ \$/min and $k_P = 28.8 \times 10^{-6}$ \$/mm².

The results of the optimum design are as follows: $n_r = 15$, $h_r = 160$, $t = 10$ mm and the total minimum cost is $K = 38964$ \$.

Comparing the ring-stiffened design with an *unstiffened* one, it is calculated that, for the unstiffened version a shell thickness of $t = 34$ mm is required. In the case considered here, where $M_x = 59.81$, $A = 58.64$, $C_P = 1.1094$, $p_{el} = 0.9761$ MPa and $1.5 \times 0.5 = 0.75 < 0.8 \times 0.9761 = 0.78$ MPa is satisfactory. The costs of the unstiffened version are as follows: $K_{F1} = 2140$ \$, $K_{F4} = 9916$ \$, $K_F = 20616$ \$, $K_M = 46535$ \$, $K_P = 10043$ \$, the total cost is $K = 77194$ \$. This is $100(77194-38964)/38964 = 98\%$ higher than that of the stiffened version.

It can be concluded that, in the case of cylindrical shells subject to external pressure, ring-stiffening is economic, since the shell is very sensitive to buckling due to external pressure.

5. Ring-stiffened cylindrical shells subject to axial compression or bending

According to DNV design rules (Det Norske Veritas [4]) the constraint on local shell buckling is expressed by

$$\sigma_{\max} \leq \sigma_{cr} = \frac{f_y}{\sqrt{1 + \lambda^4}} \quad (66)$$

$$\lambda^2 = \frac{f_y}{\sigma_E}, \quad \sigma_E = (1.5 - 50\beta) C \frac{\pi^2 E}{10.92} \left(\frac{t}{L_r} \right)^2 \quad (67)$$

$$L_r = \frac{L}{n + 1} . \quad (68)$$

The factor of $(1.5-50\beta)$ in equation (51) expresses the effect of initial radial shell deformation caused by the shrinkage of circumferential welds and can be calculated as follows (Farkas [7], Farkas & Jármai [1]).

The maximum radial deformation of the shell caused by the shrinkage of a circumferential weld is

$$u_{\max} = 0.64 A_T \sqrt{R/t}, \quad (69)$$

where $A_T t$ is the area of specific strains near the weld. According to our results (Farkas & Jármai [13])

$$A_T t = \frac{0.3355 Q_T \alpha_0}{c_0 \rho} . \quad (70)$$

For steels it is

$$A_T t = 0.844 \times 10^{-3} Q_T \quad (A_T t, \text{ in mm}^2 \quad Q_T \text{ in J/mm}), \quad (71)$$

$$Q_T = \eta_0 \frac{UI}{v_W} = C_A A_W . \quad (72)$$

For manually arc welded butt welds

$$Q_T = 60.7 A_W \quad (A_W \text{ in mm}^2) . \quad (73)$$

Here

$$A_W = \begin{cases} 10t & \text{if } t \leq 10 \text{ mm} , \\ 3.05t^{1.45} & \text{if } t > 10 \text{ mm} . \end{cases} \quad (74)$$

Introducing a reduction factor of β for which

$$0.01 \leq \beta = \frac{u_{\max}}{4\sqrt{Rt}} \leq 0.02 \quad (75)$$

the imperfection factor for shell buckling strength should be multiplied by $(1.5 - 50\beta)$.

$$\text{For } \beta \leq 0.01, \quad \beta = 0.01; \quad \text{for } \beta \geq 0.02 \quad \beta = 0.02. \quad (76)$$

$$\text{For } t > 9 \text{ mm } 1.5 - 50\beta = 1.$$

Furthermore

$$C = \psi \sqrt{1 + \left(\frac{\rho_0 \xi}{\psi}\right)^2}, \quad Z = 0.9539 \frac{L_r^2}{Rt}. \quad (77)$$

In the case of bending it is

$$\psi = 1, \quad \xi = 0.702Z, \quad \rho_0 = 0.5 \left(1 + \frac{R}{300t}\right)^{-0.5}. \quad (78)$$

In the case of axial compression

$$\psi = 1, \quad \xi = 0.702Z, \quad \rho_0 = 0.5 \left(1 + \frac{R}{150t}\right)^{-0.5}. \quad (79)$$

It can be shown that the critical buckling stress does not depend on the distance of ring stiffeners (L_r).

If

$$\rho_0 \xi > 10, \quad C \approx \rho_0 \xi = 0.702 \times 0.9539 \rho_0 \frac{L_r^2}{Rt} \quad (80)$$

and

$$\sigma_E = 0.702 \times 0.9539 \rho_0 \frac{\pi^2 Et}{10.92R} \quad (81)$$

does not depend on L_r .

From equation (80) we obtain

$$L_r > 3.8644 \sqrt{\frac{Rt}{\rho_0}}. \quad (82)$$

E.g. for $R = 1800$, $t = 18$ mm in the case of axial compression $\rho_0 = 0.3873$; $L_r > 1117$ mm, in the case of bending $\rho_0 = 0.4330$; $L_r > 1057$ mm. Therefore it can be concluded that the shell thickness can be decreased only if $L_r < 1000$ mm. This means a very dense stiffening, the welding cost of which is very high and the stiffened shell is uneconomic. The fact that the buckling strength does not depend on the shell length is first derived by Timoshenko and Gere [14].

Ring-stiffening cannot be economic for axially compressed or bent cylindrical shells, since the shell is not very sensitive to buckling for such loads, its stiffness against buckling is large. Ring-stiffening can be used to ensure the accurate cylindrical shape of the shell. In this case the designer can select a realistic domain of the number of ring-stiffeners and can search for the optimum stiffener number in this region minimizing the cost function (Farkas et al. [15]), but this minimal cost will be higher than that of an unstiffened shell.

6. A stringer-stiffened cylindrical shell loaded by bending

The shell is a supporting bridge for a belt-conveyor, simply supported with a given span length of $L = 60$ m and radius of $R = 1850$ mm (Figures 6, 7 and 8). The intensity of the factored uniformly distributed vertical load is $p = 26.0$ N/mm + self mass. Factored live load is 20.0 N/mm, dead load (belts, rollers, service-walkway) is 6.0 N/mm. For self mass a safety factor of 1.35 is used, which is prescribed by

$$\sigma_a = \frac{M}{R^2 \pi t_e} \leq \sigma_{cr} = \frac{f_y}{\sqrt{1 + \lambda^4}} \quad (83)$$

$$\lambda^2 = \frac{f_y}{\sigma_E}; \quad t_e = t + \frac{A_s}{2s}; \quad s = \frac{2R\pi}{n_s} \quad (84)$$

$$M = \frac{pL^2}{8}; \quad p = 26.0 + 1.35\rho(2R\pi t_e); \quad \rho = 7.85 \times 10^{-5} \text{ N/mm}^3 \quad (85)$$

$$\sigma_E = C(1.5 - 50\beta) \frac{\pi^2 E}{12(1 - \nu^2)} \left(\frac{t}{s}\right)^2 \quad (86)$$

$$C = 4\sqrt{1 + \left(\frac{\rho_e \xi}{4}\right)^2}; \quad Z = \frac{s^2}{Rt} \sqrt{1 - \nu^2} \quad (87)$$

$$\rho_e = 0.5 \left(1 + \frac{R}{150t}\right)^{-0.5}; \quad \xi = 0.702Z. \quad (88)$$

Note that the calculation of β is detailed in Section 5.

(2) *Stringer panel buckling*

$$\sigma_a = \frac{M}{R^2 \pi t_e} \leq \sigma_{crp} = \frac{f_y}{\sqrt{1 + \lambda_p^4}} \quad (89)$$

$$\lambda_p^2 = \frac{f_y}{\sigma_{Ep}}; \quad \sigma_{Ep} = C_p \frac{\pi^2 E}{10.92} \left(\frac{t}{L}\right)^2 \quad (90)$$

$$C_p = \psi_p \sqrt{1 + \left(\frac{0.5\xi_p}{\psi_p}\right)^2}; \quad Z_p = 0.9539 \frac{L^2}{Rt} \quad (91)$$

$$\xi_p = 0.702Z_p; \quad \gamma_s = 10.92 \frac{I_{sef}}{st^3} \quad (92)$$

$$\psi_p = \frac{1 + \gamma_s}{1 + \frac{A_s}{2s_e t}}. \quad (93)$$

Since DNV rules give the effective shell part s_e by too complicated an iteration, we use the simpler ECCS (1988) rules:

$$s_E = 1.9t \sqrt{\frac{E}{f_y}} \quad (94)$$

If $s_E < s$, $s_e = s_E$; if $s_E > s$, $s_e = s$.

I_{sef} is the moment of inertia of a cross section containing the stiffener and a shell part of width s_e

$$\begin{aligned} I_{sef} = s_e t \left(\frac{t}{2} + z_G\right)^2 + \frac{s_e t^3}{12} + \frac{t_w}{12} \left(\frac{h_1}{2}\right)^3 + \\ + \frac{h_1 t_w}{2} \left(\frac{h_1}{4} - z_G\right)^2 + \frac{bt_f^3}{12} + bt_f \left(\frac{h_1 + t_f}{2} - z_G\right)^2 \end{aligned} \quad (95)$$

$$z_G = \frac{h_1^2 t_w / 8 + h_1 b t_f / 2}{h_1 t_w / 2 + b t_f + s_e t}. \quad (96)$$

- (3) *Deflection constraint.* The moment of inertia is calculated here approximately by the formula of $\pi R^3 t_e$, while the exact expression is given by equation (132).

$$w_{\max} = \frac{5p_0 L^4}{384E\pi R^3 t_e} \leq w_{\text{allow}} = \frac{L}{\phi}; \quad \phi = 500 - 1000 \quad (97)$$

$$p_0 = 20/1.5 + 6.0/1.35 + \rho 2R\pi t_e = 17.78 + \rho 2R\pi t_e. \quad (98)$$

The selected UB rolled I-sections are given in Table 1.

Table 1. Characteristics of the selected UB rolled I-sections

UB Profile	h mm	b mm	t_w mm	t_f mm	A mm ²	$I_y \times 10^{-4}$ mm ⁴
152 × 89 × 16	152.4	88.7	4.5	7.7	2032	834
168 × 102 × 19	177.8	101.2	4.8	7.9	2426	1356
203 × 133 × 25	203.2	133.2	5.7	7.8	3187	2340
254 × 102 × 25	257.2	101.9	6.0	8.4	3204	3415
305 × 102 × 28	308.7	101.8	6.0	8.8	3588	5366
356 × 127 × 39	353.4	126.0	6.6	10.7	4977	10172
406 × 140 × 46	403.2	142.2	6.8	11.2	5864	15685
457 × 152 × 60	454.6	152.9	8.1	13.3	7623	25500
533 × 210 × 92	533.1	209.3	10.1	15.6	11740	55230
610 × 229 × 113	607.6	228.2	11.1	17.3	14390	87320
686 × 254 × 140	683.5	253.7	12.4	19.0	17840	136300
762 × 267 × 173	762.2	266.7	14.3	21.6	22040	205300
838 × 292 × 194	840.7	292.4	14.7	21.7	24680	279200
914 × 305 × 224	910.4	304.1	15.9	23.9	28560	376400

The characteristic data of the UB rolled I-sections can approximately be expressed by the main parameter of section height h (approximately equalling the first number of the profile name) as follows:

$$A_S = 1093.24394022488 + 0.0336839947h^2, \quad (99)$$

$$t_f = \sqrt{34.552565817 + 0.0006518757864h^2}, \quad (100)$$

$$b = \sqrt{4676.099669 + 0.11159269h^2}, \quad (101)$$

$$t_w = \sqrt{16.154183 + 4.228419 \times 10^{-5} h^2 \ln h}. \quad (102)$$

The cost function

Fabrication sequence:

- (1) Fabrication of 20 shell elements of length 3 m without stiffeners. For one shell element 2 axial butt welds are needed (GMAW-C) (K_{F1}). The cost of forming a shell element into the cylindrical shape is also included (K_{F0}).
- (2) Welding of an unstiffened shell unit from 4 shell segments of 3m length with 3 circumferential butt welds (K_{F2}).

- (3) Welding the n_s stiffeners to the unit with $2n_s$ fillet welds of size a_w and length 12 m (K_{F3}), $a_w = 0.3t_w$, $a_{wmin} = 3$ mm.
- (4) Welding the 5 units together with 4 butt welds and butt welds connecting the half UB stiffeners (K_{F4}).

The material cost is

$$K_M = k_{M1}5\rho_1V_2, \quad (103)$$

$$V_2 = 4V_1 + n_S \frac{A_s L}{2 \times 5}, \quad V_1 = 3000 \times 2R\pi t. \quad (104)$$

According to data obtained from a Hungarian manufacturing company (Jászberényi Aprítógépgyár, Crushing Machine Factory, Jászberény), K_{F0} can be expressed in function of shell thickness and diameter as follows (valid for $t = 4 - 40$ mm and $2R = 1500 - 3500$ mm, for width of 3000 mm)

$$K_{F0} = k_F \Theta e^\mu, \quad \mu = 6.8582513 - 4.527217t^{-0.5} + 0.009541996(2R)^{0.5}, \quad (105)$$

$$K_{F1} = k_F \left(\Theta \sqrt{\kappa \rho_1 V_1} + 1.3 \times 0.152 \times 10^{-3} t^{1.9358} \times 6000 \right), \quad (106)$$

$$\Theta = 2; \kappa = 2; \rho_1 = 7.85 \times 10^{-6} \text{kg/mm}^3,$$

$$K_{F2} = k_F \left(\Theta \sqrt{4x4\rho_1 V_1} + 1.3x0.152x10^{-3}t^{1.9358}6R\pi \right), \quad (107)$$

$$k_F = 1.0 \$/\text{min}, \quad k_{M1} = 1.0 \$/\text{kg},$$

where Θ is a difficulty factor expressing the complexity of the assembly and κ is the number of elements to be assembled.

$$K_{F3} = k_F \left(\Theta \sqrt{(n_s + 1) \rho_1 V_2} + 1.3 \times 0.3394 \times 10^{-3} a_W^2 2Ln_s/5 \right), \quad (108)$$

$$K_{F4} = k_F \left(\Theta \sqrt{5 \times 5 \rho_1 V_2} \right) + k_F 1.3x0.152x10^{-3} \left(8R\pi t^{1.9358} + n_S \frac{h_1}{2} t_w^{1.9358} + n_S b t_f^{1.9358} \right), \quad (109)$$

$$h_1 = h - 2t_f. \quad (110)$$

The cost of painting is

$$K_P = k_P \left(4R\pi L + n_s \frac{A_L L}{2} \right); \quad k_P = 14.4 \times 10^{-6} \$/\text{mm}^2, \quad (111)$$

$$A_L = 2h_1 + 4b. \quad (112)$$

The total cost is

$$K = K_M + 20K_{F1} + 20K_{F0} + 5K_{F2} + 5K_{F3} + K_{F4} + K_P. \quad (113)$$

In order to compare the stiffened shell with the unstiffened one, the constraints of an *unstiffened shell* are given as follows.

(1) *Shell buckling*

$$\sigma_b = \frac{M}{R^2 \pi t} \leq \sigma_{cr} = \frac{f_y}{\sqrt{1 + \lambda^4}}, \quad (114)$$

$$\lambda^2 = \frac{f_y}{\sigma_E}, \quad (115)$$

$$\sigma_E = C(1.5 - 50\beta) \frac{\pi^2 E}{10.92} \left(\frac{t}{L}\right)^2, \quad (116)$$

$$C = \sqrt{1 + (\rho_e \xi)^2}; \quad Z = \frac{L^2}{Rt} 0.9539, \quad (117)$$

$$\rho_e = 0.5 \left(1 + \frac{R}{300t}\right)^{-0.5}; \quad \xi = 0.702Z. \quad (118)$$

(2) *Vertical deflection*

$$w_{\max} = \frac{5p_0 L^4}{384E\pi R^3 t} \leq w_{\text{allow}} = \frac{L}{\phi}. \quad (119)$$

The cost function

Fabrication sequence:

- (1) Fabrication of 20 shell elements of length 3 m without stiffeners. For one shell element 2 axial butt welds are needed (GMAW-C) (K_{F1}). The cost of forming a shell element into the cylindrical shape is also included (K_{F0}).
- (2) Welding the 20 units together with 19 butt welds (K_{F2}).

The material cost is

$$K_M = k_{M1} 20\rho_1 V_1, \quad (120)$$

$$V_1 = 3000x2R\pi t, \quad (121)$$

$$K_{F0} = k_F \Theta e^\mu; \quad \mu = 6.8582513 - 4.527217t^{-0.5} + 0.009541996(2R)^{0.5}, \quad (122)$$

$$K_{F1} = k_F \left(\Theta \sqrt{\kappa \rho_1 V_1} + 1.3 \times 0.152 \times 10^{-3} t^{1.9358} \times 6000 \right), \quad (123)$$

$$\Theta = 2; \quad \kappa = 2; \quad \rho_1 = 7.85x10^{-6} \text{kg/mm}^3,$$

$$K_{F2} = k_F \left(\Theta \sqrt{20x20\rho_1 V_1} + 1.3 \times 0.152 \times 10^{-3} t^{1.9358} 38R\pi \right), \quad (124)$$

$$k_F = 1.0 \$/\text{min}, \quad k_{M1} = 1.0 \$/\text{kg}.$$

The cost of painting is

$$K_P = k_P (4R\pi L); \quad k_P = 14.4x10^{-6} \$/\text{mm}^2. \quad (125)$$

The total cost is

$$K = K_M + 20K_{F1} + 20K_{F0} + K_{F2} + K_P. \quad (126)$$

A numerical example using manual calculation

Assuming that the deflection constraint is active, i.e. selecting a low allowable deflection with a value of $\phi = 1000$, it is possible to determine the required thickness

of an *unstiffened* shell. From the deflection constraint – see equation (119) – one obtains an equation for the required thickness

$$t \geq \frac{5L^3\phi}{384E\pi R^3} (17.78 + \rho 2R\pi t) . \quad (127)$$

For $L = 60$ m, $R = 1850$ mm, $E = 2.1 \times 10^5$ MPa, $\phi = 1000$, $\rho = 7.85 \times 10^{-5}$ N/mm³

$$t \geq 0.6733 (17.78 + 0.9125t) . \quad (128)$$

Solving this equation we get $t = 32$ mm.

Checking this unstiffened shell for buckling we obtain the following values – see equations (114-118): $p = 65.42$ N/mm, $M = 29.439 \times 10^9$ Nmm, $\sigma_{\max} = 85.56$ MPa, $Z = 58.01 \times 10^3$, $\xi = 40.72 \times 10^3$, $\rho_e = 0.4578$, $C = 18642$, $\sigma_E = 1006$ MPa, $\sigma_{cr} = 334.8 > 85.56$ MPa, OK.

The cost calculation of the unstiffened shell results in the following values – see equations (120-126): $V_1 = 1.1159 \times 10^9$ mm³, $K_M = 175195$ \$, $K_{F0} = 1528$ \$, $K_{F1} = 1159$ \$, $K_{F2} = 39517$ \$, $K_P = 20086$ \$, the total cost is $K = 288538$ \$.

Calculation of a stringer-stiffened shell with the same deflection constraint. Equation (128) results in a formula for t_e

$$t_e \geq 0.6733 (17.78 + 0.9125t_e) \quad (129)$$

which gives $t_e = 32$ mm. t_e contains all the three unknowns (t , n_s , A_s)

$$t_e = t + \frac{n_s A_s}{4R\pi} \quad (130)$$

since we use for a stiffener only the half cross-section of a rolled I-section ($A_s/2$).

For the minimum cost solution we need a mathematical algorithm, but, to show the cost savings achieved by decrease of the unstiffened shell thickness of 32 mm, we use a manual calculation and take $t = 10$ mm. If we select a rolled I-section of UB 914 \times 305 \times 289 ($A_s = 36830$ mm²), then the required number of stiffeners from equation (130) is $n_s = 10$.

The selected UB section has the following dimensions: $h = 926.6$, $h_1 = 862.6$, $b = 307.7$, $t_w = 19.5$, $t_f = 32$ mm, the half surface for the calculation of painting cost is $A_L/2 = 1506$ mm²/mm.

Note that this UB profile is not included in Table 1.

Checking the stringer-stiffened shell for buckling using equations (83-88).

$p = 38.318$ N/mm, $M = 172.43 \times 10^8$ Nmm, $\sigma_{\max} = 62$ MPa, $s = 1162$ mm, $Z = 69.62$, $\xi = 48.87$, $\rho_e = 0.3346$, $C = 16.83$, $\sigma_E = 237$ MPa, $\sigma_{cr} = 197 > 62$ MPa, OK.

Check of stringer panel buckling using equations (89-96) .

$s_e = 642$ mm, $z_0 = 264.9$ mm, $I_{sef} = 7.476 \times 10^8$ mm⁴, $\gamma_s = 7025.6$, $\psi = 1409.3$, $\rho_e = 0.5$, $Z = 185.6 \times 10^3$, $\xi = 130310$, $C = 65166$, $\sigma_E = 343.6$ MPa, $\sigma_{cr} = 247 > 62$ MPa, OK.

Check of deflection. The exact calculation of the moment of inertia for the deflection uses the following formulae (Figure 8):

The distance of the center of gravity for the half UB section is

$$z_A = \frac{h_1 t_w / 2 (h_1 / 4 + t_f / 2)}{h_1 t_w / 2 + b t_f} \quad (131)$$

The moment of inertia of the half UB section is expressed by

$$I_x = b t_f z_A^2 + \frac{t_w}{12} \left(\frac{h_1}{2} \right)^3 + \frac{h_1 t_w}{2} \left(\frac{h_1}{4} - z_A \right)^2 \quad (132)$$

The moment of inertia of the whole stiffened shell cross-section is

$$I_{x0} = \pi R^3 t + I_x \sum_{i=1}^{n_s} \sin^2 \left(\frac{2\pi i}{n_s} \right) + \left(\frac{h_1 t_w}{2} + b t_f \right) \left(R + \frac{h_1 + t_f}{2} - z_A \right)^2 \sum_{i=1}^{n_s} \sin^2 \left(\frac{2\pi i}{n_s} \right) \quad (133)$$

In our case $z_A = 106.7$ mm, $I_x = 3.83 \times 10^8$ mm⁴, $I_{x0} = I_x + (1.989 + 4.400)10^{11} = 6.393 \times 10^{11}$ mm⁴, $p_0 = 41.36$ N/mm.

The approximate formula for the moment of inertia gives a smaller value of $I_{x0} \approx \pi R^3 t_e = 5.14 \times 10^{11}$ mm⁴ because, with equation (130) $t_e = 25.84$ mm.

The exact deflection is $w_{\max} = \frac{5p_0 L^4}{384EI_{x0}} = 52 < 60$ mm, OK.

It can be concluded that the approximate formula of I_{x0} gives a value on the safe side. Note that, in the case of inside half UB section stiffeners, this approximate formula overestimates the exact value, thus, outside stiffeners are more effective than inside ones.

Cost calculation of the stiffened shell using equations (103-113).

$V_1 = 3.4872 \times 10^8$ mm³, $V_2 = 3.6047 \times 10^9$ mm³, $K_M = 141485$ \$, $K_{F0} = 812.55$ \$, $K_{F1} = 250.3$ \$, $K_{F2} = 1012$ \$, $K_{F3} = 1497$ \$, $K_{F4} = 3241$ \$, $K_P = 33098$ \$, the total cost is $K = 211628$ \$, i.e. stringer stiffening results in 36% cost savings. It should be mentioned that the cutting costs of UB sections can be neglected.

Comparison of the costs for unstiffened and stiffened shells

This comparison is shown in Table 2.

Table 2. Summary of costs (negative difference means cost savings)
(Costs in \$)

Cost	Unstiffened shell	Stiffened shell	Difference %
Material K_M	175195	141485	-24
Forming K_{F0}	30560	16251	-88
Welding $20K_{F1} + K_{F2}$	62697		
Welding $20K_{F1} + 5K_{F2} + 5K_{F3} + K_{F4}$		20794	-201
Painting K_P	20086	33098	64
Total	288538	211628	-36

It can be seen that the cost savings caused by stringer stiffening are significant in forming and welding costs, but painting for an unstiffened shell is 64% cheaper than that for a stiffened one. It can be concluded that the cost factors of fabrication and painting play an important role in the achievable cost savings.

7. Conclusions

The economy of stiffening is characterized by a cost comparison of stiffened and unstiffened structural versions. For this purpose the own cost calculation method is used, which is developed mainly for welded structures. The cost function includes the costs of material, forming of shell elements into cylindrical shape, assembly, welding and painting and is formulated according to the fabrication sequence.

The economy of stiffening depends on type of structure (plate, cylindrical shell), type of stiffening (rings, stringers), stiffener profile (flat, L-, trapezoidal, rolled I-section etc.), loading (axial compression, bending, external pressure), constraints (buckling, deflection). Therefore the cost comparison is performed for the following cases: (a) a longitudinally stiffened plate loaded by axial compression, (b) an orthogonally stiffened square plate with transverse loading, (c) a ring-stiffened shell subject to external pressure, (d) a ring-stiffened shell loaded by axial compression or bending, (e) a stringer-stiffened shell loaded by bending with a deflection constraint.

Summarizing the above cost comparisons it can be concluded that the economy of these structures shows the following differences:

- (1) stiffened plates are always economic, since they are very sensitive to buckling and transverse deflection;
- (2) ring-stiffened cylindrical shells are economic only in the case of external pressure, but for axial compression and bending they are uneconomic and can be used only to guarantee the appropriate cylindrical shape;
- (3) cylindrical shells stiffened outside by stringers are economic for bending with an active deflection constraint, but for axial compression or bending without a deflection constraint they are uneconomic. In order to decrease the welding cost, the stiffeners should have a cross-sectional area as large as possible and should be welded to the shell with welds as small as possible, thus halved rolled I-section stringers are advantageous for this purpose.

Acknowledgement. This research has been supported by the Hungarian Scientific Research Foundation grants OTKA T 38058 and T 37941. Special thanks are due to my colleague Prof. Dr. Károly Jármai co-author of optimum design problems applied in this review article.

References

1. FARKAS, J. and JÁRMAI, K.: *Economic design of metal structures*. Millpress Science Publisher, Rotterdam, 2003.
2. American Petroleum Institute (API) Bulletin 2U. *Bulletin on stability design of cylindrical shells*. 2nd ed. Washington, 2000.
3. European Convention of Constructional Steelwork (ECCS), *Recommendations for Steel Construction. Buckling of steel shells*. No.56. Brussels, 1988.

4. Det Norske Veritas (DNV), *Buckling strength analysis*. Classification Notes No.30.1. Hovik, Norway, 1995.
5. MIKAMI, I. and NIWA, K.: Ultimate compressive strength of orthogonally stiffened steel plates. *J. Struct. Engng ASCE*, **122**(6), (1996), 674-682. Discussion by Bedair, O. and authors' closure. *J. Struct. Engng*, **123**(7), (1997), 1116-1119.
6. *Stahlbau Handbuch, Band 2.*, Köln, Stahlbau-Verlag, 1985.
7. FARKAS, J.: Thickness design of axially compressed unstiffened cylindrical shells with circumferential welds. *Welding in the World*, **46**(11/12), (2002), 26-29.
8. SCHADE, H. A.: Design curves for cross-stiffened plating under uniform bending load. *Trans. Soc. Nav. Arch. and Marine Engrs*, **49**, (1941), 154-182.
9. TIMOSKENKO, S. and WOINOWSKY-KRIEGER, S.: *Theory of Plates and Shells*. 2nd ed. New York, McGraw Hill, 1959.
10. FARKAS, J. and JÁRMAI, K.: *Analysis and Optimum Design of Metal Structures*. Balkema, Rotterdam-Brookfield, 1997.
11. VOLMIR, A. S.: 1967. *Buckling Strength of Deformable Systems*. Moscow, Nauka, 1967. (in Russian)
12. Eurocode 3. *Design of steel structures*. Part 1.1. General rules and rules for buildings. European Prestandard ENV 1993-1-1. CEN European Committee for Standardisation, Brussels, 1992.
13. FARKAS, J. and JÁRMAI, K.: Analysis of some methods for reducing residual beam curvatures due to weld shrinkage. *Welding in the World* **41**(4), (1998), 385-398.
14. TIMOSHENKO, S. P. and GERE, J. M.: *Theory of elastic stability*. 2nd ed. New York, Toronto, London, McGraw Hill, 1961.
15. FARKAS, J., JÁRMAI, K. and VIRÁG, Z.: Optimum design of a belt-conveyor bridge constructed as a welded ring-stiffened cylindrical shell. IIW-Doc. XV-WG9-23-03, XV-1144-03. Bucharest, 2003.

MICROHARDNESS TESTS OF GRADED SiC/EP RINGS: EXPERIMENTAL RESULTS AND FE MODELING

DÁVID FELHŐS, KÁROLY VÁRADI

Institute of Machine Design
Budapest University of Technology and Economics
Műegyetem rkp. 3, 1111 Budapest, Hungary
varadik@goliat.eik.bme.hu

KLAUS FRIEDRICH

Institute for Composite Materials (IVW GmbH.)
Technical University of Kaiserslautern, Erwin-Schrödinger-Strasse
67663 Kaiserslautern, Germany
klaus.friedrich@ivw.uni-kl.de

[Received: January 22, 2005]

Dedicated to István Páczelt on the occasion of his 65th birthday

Abstract. Ring-shaped test specimens were made of gradient-structured SiC/EP composite produced by centrifugation. Compression tests and microhardness measurements were performed on epoxy matrix composites of even distribution of SiC reinforcement particles in various degrees of vol.%. As a result, compression stress-strain curves were obtained for the composites as well as changes of universal hardness in function of the SiC vol.% in order to have data for the material properties of the layers of the functionally grade structures. Microhardness measurements were simulated by 2D axisymmetrical and 3D FE micro-models in order to reveal the impact of reinforcement particles on material behavior, i.e. to explore the stresses and strains in the vicinity of the indented area as well as to find how functionally graded materials improve the wear resistance of composites.

Mathematical Subject Classification: 74M25, 74S05

Keywords: microhardness test, functionally graded material, FE analysis

1. Introduction

Functionally gradient materials (FGM) are characterized by the fact that one component is not evenly dispersed in the other component. One of them, the matrix, is usually a thermosetting or thermoplastic polymer; the other, the reinforcement material is a short fiber, metal or ceramic particle. Due to their good wear characteristics, FG materials are intended to be used for rollers, gears, driving and sliding rings, whose wear characteristics are better than those with identical material composition but made from a composite of even material distribution [1, 2]. Depending on the material composition, characteristics changing with gradient features include mechanical, thermal, electrical, magnetic, optical, or other properties [3].

Microhardness tests provide important features to forecast the wear characteristics of a material. FE calculations are suitable for identifying the stresses in a micro-environment, enabling us to gain a deeper knowledge of the expected behavior of different materials.

The object of our research is an FG composite material containing SiC reinforcement particles distributed in an epoxy matrix. The following models are aimed at exploring the contact, stress, and deformation processes in the micro-environment of the material in the course of microhardness measurements. While modeling microhardness measurements, the behavior of a composite of even material distribution containing pure resin and 20 vol.% SiC particles was studied in order to explore the load transfer mechanism of the reinforcement particles.

2. Experimental

2.1. Materials and processes. In the present study, a SiC/EP composite was examined with the material properties listed in Table 1. The matrix was cured with an amine hardener. The reinforcement particles are of irregular forms with coarse edges (Figure 1).

Table 1. Data of the matrix and reinforcement particles

Name	Producer	Density [g/cm ³]	Elastic modulus [GPa]	Size [μm]
Matrix: High-temperature epoxy resin:	Vantico	1.8	2.654	
Filler: Silicon carbide, SiC	Mineralien-Werke Kuppenhaim GmbH	3.2	455	9

In order to reach an even material distribution within the composite, the particles were distributed in the matrix by a dissolver (Dispermat AE, VMA-Getzmann

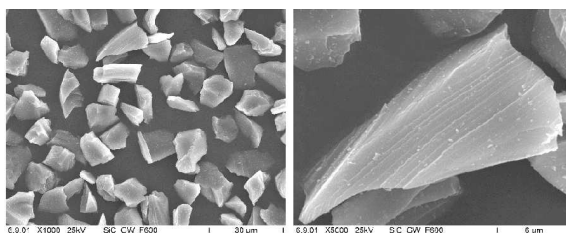


Figure 1. SEM images of SiC reinforcement particles in an epoxy matrix GmbH). A composite containing 5 vol.% of reinforcement particles was used for producing gradient rollers, which were cured in a cylindrical mould. The gradient nature of SiC particle distribution was achieved by centrifugation of the mix at 1000 1/min velocity for 30 minutes (Figure 2).

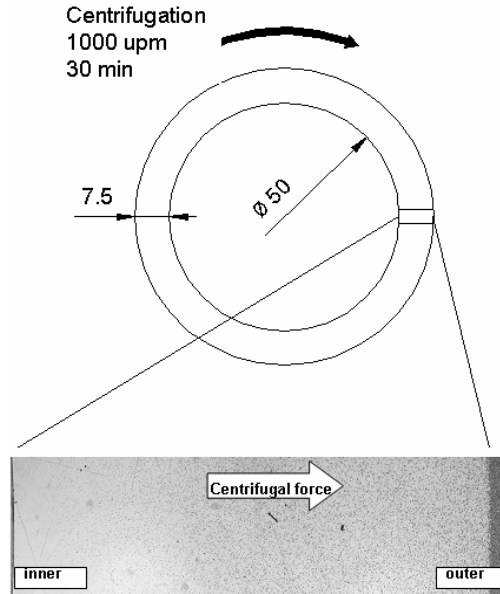


Figure 2. Preparation of FG-structured material

2.2. Microhardness tests. Microhardness tests were performed along the cross-section of the gradient roller (Figure 2) and on test pieces of even SiC distribution in various degrees of vol.%. Measurements were taken by a Shimadzu DUH-202 microhardness measurement device at room temperature, using a Vickers indenter, at 100 MN and 1500 MN of loading force, with an identical loading and unloading velocity of 70 mN/s and 2 sec of follow-up load. The loading force was chosen to be 1500 MN in the course of the measurements performed to identify the material distribution of the gradient roller; a loading force of 100 MN was chosen for the reference measurements of FE models to compare the size of displacements and the largest size of reinforcement particles in order to study the local behavior of specific particles.

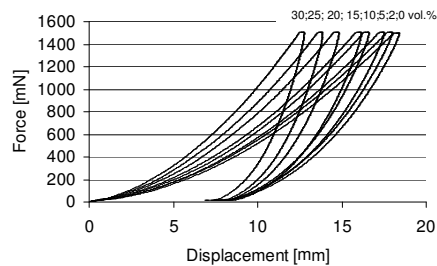


Figure 3. Force vs. displacement curves of microhardness measurements for different vol.% of SiC particles

Due to the high loading force (1500 MN), fairly large indentations were produced (of 90 to 120 μm), so that we could receive an average hardness value characterizing the composite as well as elastic modulus values from the unloading curves of force vs. displacement.

First, measurements were performed on test pieces of even SiC particle distribution for various degrees of vol.%, in order to arrive at a curve of universal hardness in the function of the vol.% of reinforcement particles. Ten measurements were performed for each characteristic vol.% value. The characteristic vol.% series are as follows: 0-, 2-, 5-, 10-, 15-, 20-, 25-, 30-vol.%. Figure 3 shows these curves of force vs. displacement. It can be observed that vol.% values change the results in approximately identical degrees.

Universal hardness HU can be calculated as [4]:

$$HU = \frac{F}{26,43h^2} \text{ [MPa]} \quad (1)$$

where F is the measuring force [N] and h is the depth of the indentation [mm]. Figure 4 shows changes in universal hardness HU in the vol.% of SiC particles.

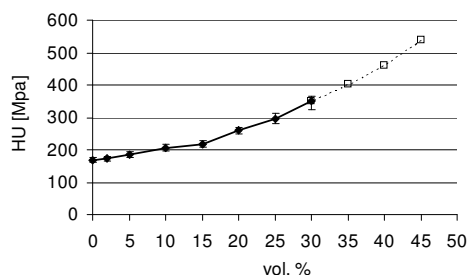


Figure 4. Universal hardness in the function of the SiC vol.%

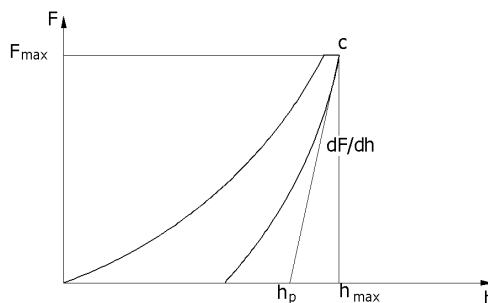


Figure 5. Elastic modulus calculation from the unloading section of the force vs. displacement curve of the hardness measurement

Hardness measurement provides a basis for determining the elastic modulus of a composite containing a given vol.% of SiC. The elastic modulus E can be calculated from the tangent of the unloading curve and the depth of the indentation (Figure 5)

by the following equations:

$$E = \left(\frac{\pi}{A}\right)^{\left(\frac{1}{2}\right)} \frac{S}{2} (1 - \nu^2), \quad (2)$$

$$A = 24.5h^2, \quad (3)$$

$$S = (dF/dh)|_{h_{\max}} \quad (4)$$

where A is the projected area of the indentation, S is the initial tangent of the unloading curve and ν is the Poisson's ratio of the material examined [5].

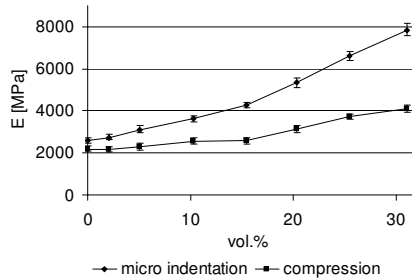


Figure 6. Compression elastic module values resulting from microhardness and compression tests in function of the SiC vol.%

Figure 6 shows the elastic modulus calculated from microhardness measurements for different vol.% of reinforcement particles and also obtained from the compression test. It can be observed that as the vol.% of reinforcement particles increases, the elastic modulus also increases. The higher elastic modulus values of microhardness tests are probably due to the different deformation mechanisms in the cases of microhardness and compression tests. It is likely that for the compression test the matrix can more uniformly deform than the local material structure in the case of microhardness

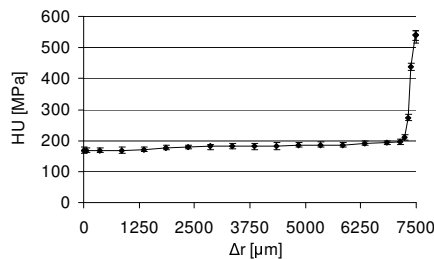


Figure 7. Universal hardness along the cross-section of an FG roller (see Figure 2)

tests. In the latter case the linking of particles, during the load transfer produces a higher local stiffness because mainly a few, partly connected particles transfer the load. Similar tendencies are reported in [1], where the microhardness test produced also higher elastic modulus values than the DMTA test at increasing vol.% of SiC particles.

2.3. Determination of the SiC volume content along the cross-section of a gradient roller. Using the values of universal hardness HU measured at test pieces of uniform particle distribution, a master curve was drawn (Figure 4), in the function of different SiC content. This master curve can be used to predict the SiC content of the layers of the cross-section of the gradient roller from the values of universal hardness HU measured in each layer (Figure 7).

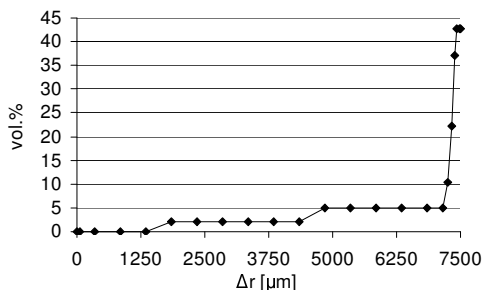


Figure 8. The SiC vol.% along the cross-section of an FG roller. Thus, we can arrive at the vol.% distribution of reinforcement particles in the cross-section of the FG roller (Figure 8). In the course of microhardness measurements along the cross-section of the gradient roller, the gradient nature of the roller can be specified with proper approximation if sufficiently small intervals are selected. A similar indirect method was applied by Watanabe et al. [6] to determine the distribution of aluminum fibers in their ceramic composite of gradient material distribution. In our measurements we observed that reinforcement particles almost entirely moved away from the inner part of the roller, while they came to around in more than 40 vol.% along the outer diameter. Therefore, centrifugation is a procedure suitable for achieving the largest possible vol.% of reinforcement particles.

2.4. Mechanical characteristics of the homogeneous EP/SiC composite. Compression tests were performed on cylindrical test specimens made of the material

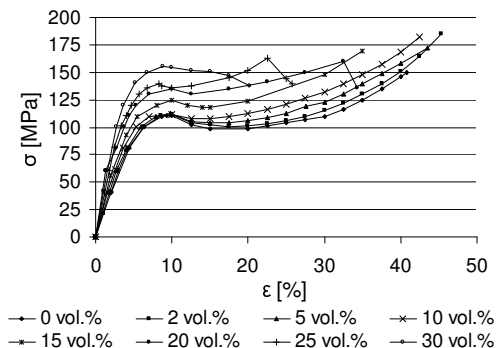


Figure 9. Compression stress-strain curves at characteristic vol.% values

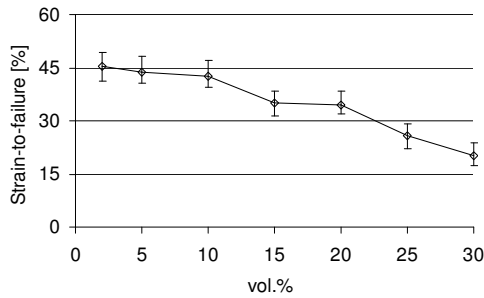


Figure 10. Maximum strain-to-failure values in the function of the SiC vol.%

of the gradient roller, with even material distribution but at varying vol.% values. The compression stress-strain curves of the EP/SiC composites have been required as compression load is characteristic for rollers as well as pressure is the dominant form of load in the course of microhardness tests as well. The compression stress-strain curves in function of the SiC vol.% are presented in Figure 9. Pure resin (0 vol.%) can bear fairly large strains. As regards the compression strength, it can be observed that as the SiC vol.% increases, the compression strength will slightly decrease. The great strain-to-failure ratio of the composite gradually reduces as the SiC vol.% increases (Figure 10).

3. FE modeling and results

3.1. The axisymmetrical FE model. An axisymmetrical model with contact elements was prepared using non-linear material properties.

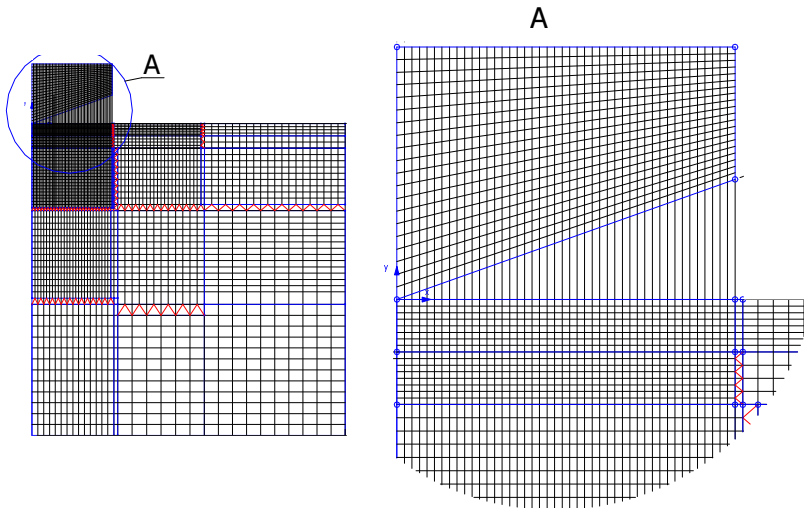


Figure 11. The FE mesh of the axisymmetrical model

Figure 11 shows the FE mesh. Load is introduced at the bottom of the model in the form of pressure, while the nodes at the upper plane of the diamond pyramid are fixed. The plane angle of the Vickers indenter had to be changed because in the axisymmetrical model the indenter is a cone rather than a pyramid. The condition of an equivalent cone angle is to have the same projected area when the indenter is pressed in the same depth. The angle of the cone results in 19.517° . The models include 3903 nodes, 6303 PLANE2D elements, and 56 contact elements. Its dimensions are: $\emptyset 80 \mu\text{m} \times 40 \mu\text{m}$. Calculations for the composite material containing 20 vol.% SiC are non-linear (material law is according to Figure 9), force control driven, applying the Newton-Raphson solution technique. The maximum load applied was 100 MN.

3.2. The 3D FE micro- model. The reinforcement particles as regular micro-cubes are embedded in the matrix, representing 20 vol.% of SiC (Figure 12).

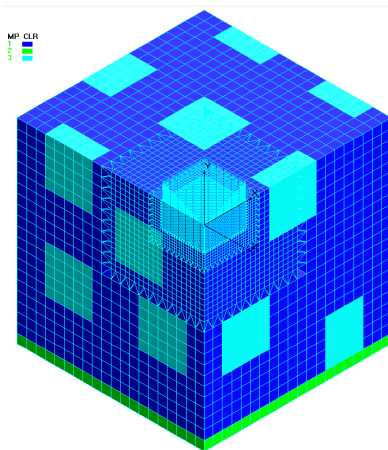


Figure 12. 3D micro-model representing 20 vol.% of SiC

In the model the diamond pyramid is connected to the test specimen by contact elements. Load is introduced from the bottom of the model. Nodes at the top of the indenter are fixed. A non-linear material law was applied for the matrix according to the compression stress-strain curve (Figure 10), while the particles were assumed to be linear elastic. The model contains 50,907 nodes, 59,357 SOLID elements and 1579 contact elements. Its dimensions are: $39.875 \times 39.875 \times 42 \mu\text{m}$. Calculations are non-linear, force control driven, applying the Newton-Raphson solution technique. The CPU time was approx. 16 hours on a P4 machine.

3.3. FE results for the composite containing of 20 vol.% SiC. The axisymmetrical model has a homogeneous material structure. Basic differences can be observed when comparing the stress and strain results of the axisymmetrical and 3D micro-models (Figure 13). The 3D micro-models are only capable of depicting the contact state more accurately between the contacting bodies because of the pyramid shape of the diamond indenter.

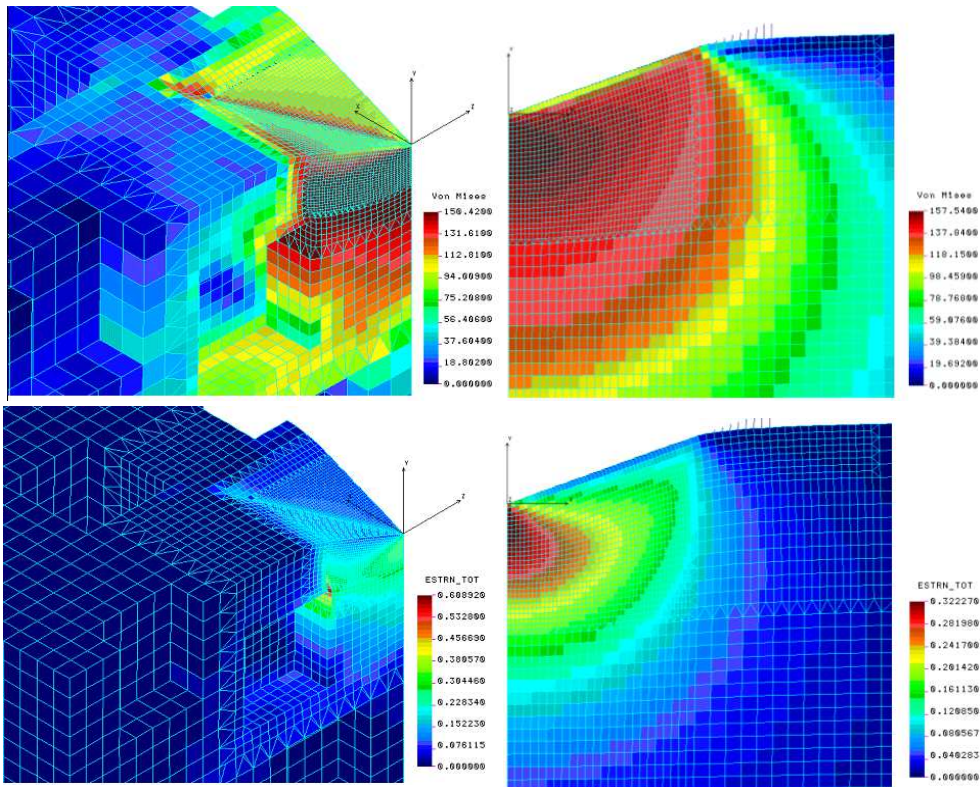


Figure 13. Von Mises equivalent stress (a) and equivalent strain (b) results in the vicinity of the contact area in the case of the 3D and axisymmetrical models

According to the axisymmetrical model the contact pressure distribution (σ_y in Figure 14) is nearly uniform along the contact area. The Von Mises equivalent stress is practically constant due to the extensive plastic deformation in the vicinity of the

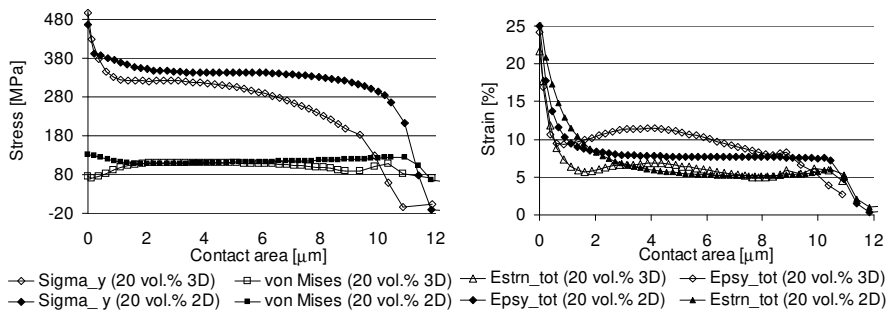


Figure 14. Stress (a) and strain (b) results along the contact area

contact area. As regards the 3D micro-model, a considerable difference can be observed in the stress and strain distribution over the contact area, depending on the fact whether the results represent the side-plane of the diamond pyramid or the edge of the pyramid (“diagonal” in Figure 15).

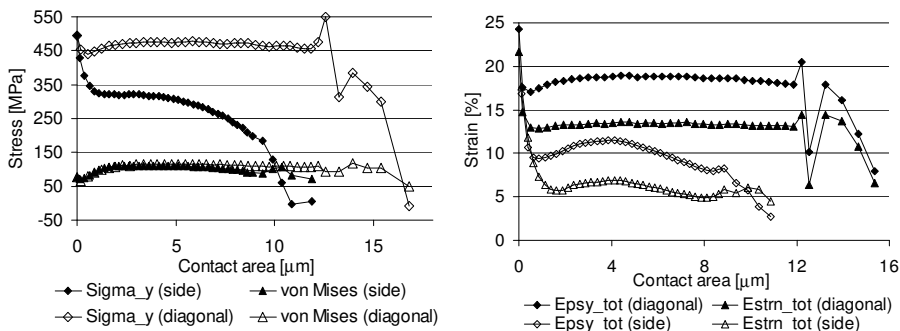


Figure 15. Stress (a) and strain (b) results in the contact area of the 3D micro-model considering the side of the indenter and its edges (called ‘diagonal’)

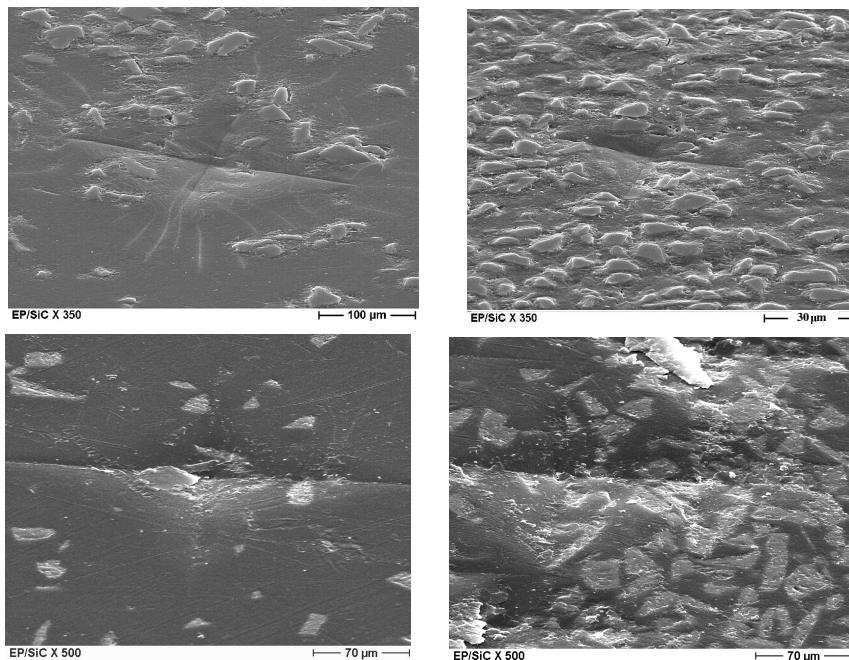


Figure 16. SEM images of microhardness measurement

Larger stresses and strains are produced along the edges of the pyramid, therefore the matrix can be damaged there, as shown by the SEM images (Figure 16). Accordingly, microcracks may be produced in the matrix along the edges.

The 3D micro-model, in Figure 13 clearly shows the behavior of SiC particles in the matrix. The highest stress peak and the largest strain are produced at the edges of the reinforcement particle. Destruction in the surroundings of the highly loaded particles is also proven by the SEM images (Figure 16). This is not transferred to the deeper layers of the material. It can be observed below the contact area that reinforcement particles touch each other at their edges and transmit the load to each other (Figure 17). In such cases, load is transmitted to the matrix through the embedded surface of connecting particles and therefore even less stress and strain is produced therein. In the same time this ‘connection’ produces a stiffer behavior locally (see Section 2.2).

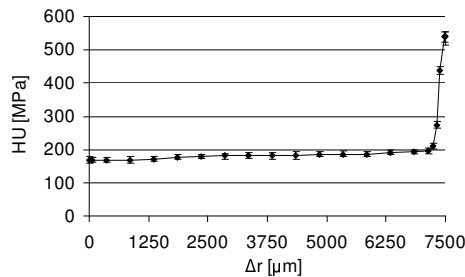


Figure 17. The “linking” of particles during load transfer

Finally, comparing the force vs. displacement curves of the microhardness measurements performed with the force vs. displacement curves taken from the results of the axisymmetrical and 3D FE micro-models, excellent agreement can be found (Figure 18).

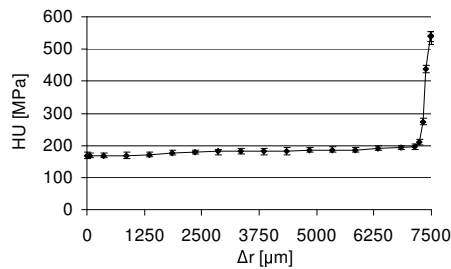


Figure 18. Comparison of the force-displacement results of the measurement and FE models

According to the results of the FE model, it can be assumed that the matrix among reinforcement particles on the surface can crack down or wear off in the wear process, but particles embedded in the matrix relatively deeply and along a larger surface area stay on the surface and produce a wear-resistant surface. This wear-resistance feature can only be produced if the reinforcement particles are located so densely beside each

other on the surface that they are connected to each other and can transfer stress to each other. Therefore this dense configuration can reduce the overloading of single particles.

4. Conclusions

The FE results according to the 2D axisymmetrical and 3D micro-models show a good correlation with the force vs. displacement results of microhardness tests in spite of the fact that in the case of axisymmetrical models a conical indenter is modeled instead of a pyramid one.

Based on the 3D micro-model, a primary stress concentration is generated in the matrix at the edges of the diamond and at the edges of reinforcement particles.

Reinforcement particles distribute load along a larger surface area within the matrix, thereby also improving its wear-resistance. The particles in a large volume fraction produce a nearly uninterrupted structure in the matrix.

According to SEM images as well as calculation results, the matrix is damaged at the surface and at the edges of particles. In the course of the wear process, the matrix among the particles probably wear off from the surface, but well-embedded particles mainly remain at their places and reduce further wear.

References

1. KRUMOVA, M., KLINGSHIRN, C. HAUPERT, F. and FRIEDRICH, K.: Microhardness studies of functionally graded polymer composites. *Compos. Sci. Techn.*, **61**, (2001), 557–563.
2. KLINGSHIRN, C., KOIZUMI, M., HAUPERT F., GIERTZSCH, H. and FRIEDRICH, K.: Structure and wear of centrifuged epoxy-resin/carbon fiber functionally graded materials *J. Mater. Sci. Let.*, **19**, (2000), 263–266.
3. HIRAI, T.: Functionally graded materials in "Materials science and technology: a comprehensive treatment", Cahn, R. W. (ed.). (Weinheim: VCH Verlagsgesellschaft GmbH 1996), 295–337.
4. Deutsche Norm: Prüfung metallischer Werkstoffe, Universelhärteprüfung, Teil 1. Prüfverfahren DIN 50359-1: 1997 – 10.
5. OLIVER, W. C. and PHARR G. M.: An improved technique for determining hardness and elastic modulus using load and displacement sensing indentation experiments. *J. Mater. Res.*, **7**, (1992), 1564–1583.
6. WATANABE, Y. and FUKUI Y.: Fabrication of functionally-graded aluminum materials by the centrifugation method. *Aluminium Transactions*, **2**, (2000), 195-208.

Notes for Contributors

to the Journal of Computational and Applied Mechanics

Aims and scope. The aim of the journal is to publish research papers on theoretical and applied mechanics. Special emphasis is given to articles on computational mechanics, continuum mechanics (mechanics of solid bodies, fluid mechanics, heat and mass transfer) and dynamics. Review papers on a research field and materials effective for teaching can also be accepted and are published as review papers or classroom notes. Papers devoted to mathematical problems relevant to mechanics will also be considered.

Frequency of the journal. Two issues a year (approximately 80 pages per issue).

Submission of Manuscripts. Submission of a manuscript implies that the paper has not been published, nor is being considered for publication elsewhere. Papers should be written in standard grammatical English. Two copies of the manuscript should be submitted on pages of A4 size. The text is to be 130 mm wide and 190 mm long and the main text should be typeset in 10pt CMR fonts. Though the length of a paper is not prescribed, authors are encouraged to write concisely. However, short communications or discussions on papers published in the journal must not be longer than 2 pages. Each manuscript should be provided with an English Abstract of about 50–70 words, reporting concisely on the objective and results of the paper. The Abstract is followed by the Mathematical Subject Classification – in case the author (or authors) give the classification codes – then the keywords (no more than five). References should be grouped at the end of the paper in numerical order of appearance. Author's name(s) and initials, paper titles, journal name, volume, issue, year and page numbers should be given for all journals referenced.

The journal prefers the submission of manuscripts in \LaTeX . Authors should prefer the $\mathcal{AMS}\text{-}\text{\LaTeX}$ article class and are not recommended to define their own \LaTeX commands. Visit our home page for further details concerning the issue how to edit your paper.

For the purpose of refereeing, two copies of the manuscripts should initially be submitted in hardcopy to an editor of the journal. The eventual supply of an accepted-for-publication paper in its final camera-ready form (together with the corresponding files on an MS-DOS diskette) will ensure more rapid publication. Format requirements are provided by the home page of the journal from which sample \LaTeX files can be downloaded:

<http://www.uni-miskolc.hu/home/web/pumns/mechanics>

These sample files can also be obtained directly (via e-mail) from a member of the Editorial Board, Gy. Szeidl (Gyorgy.SZEIDL@uni-miskolc.hu), upon request.

Twenty offprints of each paper will be provided free of charge and mailed to the correspondent author.

The Journal of Computational and Applied Mechanics is abstracted in Zentralblatt für Mathematik and in the Russian Referativnij Zhurnal.

Responsible for publication: Rector of the Miskolc University

Published by the Miskolc University Press under the leadership of Dr. József PÉTER

Responsible for duplication: works manager Mária KOVÁCS

Number of copies printed: 200

Put to the Press on February 27, 2006

Number of permission: TU 2006-300-ME

HU ISSN 1586–2070

A Short History of the Publications of the University of Miskolc

The University of Miskolc (Hungary) is an important center of research in Central Europe. Its parent university was founded by the Empress Maria Teresia in Selmecebánya (today Banská Štiavnica, Slovakia) in 1735. After the first World War the legal predecessor of the University of Miskolc moved to Sopron (Hungary) where, in 1929, it started the series of university publications with the title *Publications of the Mining and Metallurgical Division of the Hungarian Academy of Mining and Forestry Engineering* (Volumes I.-VI.). From 1934 to 1947 the Institution had the name Faculty of Mining, Metallurgical and Forestry Engineering of the József Nádor University of Technology and Economic Sciences at Sopron. Accordingly, the publications were given the title *Publications of the Mining and Metallurgical Engineering Division* (Volumes VII.-XVI.). For the last volume before 1950 – due to a further change in the name of the Institution – *Technical University, Faculties of Mining, Metallurgical and Forestry Engineering, Publications of the Mining and Metallurgical Divisions* was the title.

For some years after 1950 the Publications were temporarily suspended.

After the foundation of the Mechanical Engineering Faculty in Miskolc in 1949 and the movement of the Sopron Mining and Metallurgical Faculties to Miskolc, the Publications restarted with the general title *Publications of the Technical University of Heavy Industry* in 1955. Four new series - Series A (Mining), Series B (Metallurgy), Series C (Machinery) and Series D (Natural Sciences) - were founded in 1976. These came out both in foreign languages (English, German and Russian) and in Hungarian.

In 1990, right after the foundation of some new faculties, the university was renamed to University of Miskolc. At the same time the structure of the Publications was reorganized so that it could follow the faculty structure. Accordingly three new series were established: Series E (Legal Sciences), Series F (Economic Sciences) and Series G (Humanities and Social Sciences). The latest series, i.e., the series H (European Integration Studies) was founded in 2001. The eight series are formed by some periodicals and such publications which come out with various frequencies.

Papers on computational and applied mechanics were published in the

Publications of the University of Miskolc, Series D, Natural Sciences.

This series was given the name Natural Sciences, Mathematics in 1995. The name change reflects the fact that most of the papers published in the journal are of mathematical nature though papers on mechanics also come out.

The series

Publications of the University of Miskolc, Series C, Fundamental Engineering Sciences

founded in 1995 also published papers on mechanical issues. The present journal, which is published with the support of the Faculty of Mechanical Engineering as a member of the Series C (Machinery), is the legal successor of the above journal.



Contents
Contributed Papers

Gyula BÉDA: Generalized Mindlin's method for the determination of constitutive equations of solids	153–158
Anikó CSÉBFALVI: Evolution methods for discrete minimal weight design of space trusses with stability constraints	159–173
István ECSEDI and Kornél DLUHI: A reciprocal theorem for steady-state heat conduction problems	175–182
József FARKAS: Economy of welded stiffened steel plates and cylindrical shells	183–205
Dávid FELHŐS, Károly VÁRADI and Klaus FRIEDRICH: Microhardness tests of graded SIC/EP rings: experimental results and FE modeling	207–218
Dezső HEGYI and Krisztián HINCZ: Long-term analysis of prestressed membrane structures	219–235
Károly JÁRMAI: Particle swarm method as a new tool for structural optimization	237–256
Imre KOZÁK: Tensors of finite rotations and small strains on the middle surface of a shell	257–276
András LENGYEL and Zsolt GÁSPÁR: Compatibility paths of an infinitely degenerate mechanism	277–284
Lidia NAZARENKO: Three-component discretely-fibrous composites under matrix microdamaging	285–294
Yaroslav A. ZHUK and Igor K. SENCHENKOV: Investigation of energy characteristics of the layered beam-damper	295–309
Olaf WECKNER and Etienne EMMRICH: Numerical simulation of a non-local bar	311–319